

Article

Evaluation of Global Decametric-Resolution LAI, FAPAR and FVC Estimates Derived from Sentinel-2 Imagery

Qiong Hu ¹, Jingya Yang ², Baodong Xu ^{2,3,*} , Jianxi Huang ^{4,5} ,
Muhammad Sohail Memon ^{6,7} , Gaofei Yin ^{8,9}, Yelu Zeng ¹⁰ , Jing Zhao ³  and Ke Liu ¹¹

¹ Key Laboratory for Geographical Process Analysis & Simulation of Hubei Province/School of Urban and Environmental Sciences, Central China Normal University, Wuhan 430079, China; huqiong@mail.ccnu.edu.cn

² Macro Agriculture Research Institute, College of Resources and Environment, Huazhong Agricultural University, Wuhan 430070, China; jingya.yang@webmail.hzau.edu.cn

³ State Key Laboratory of Remote Sensing Science, Aerospace Information Research Institute, Chinese Academy of Sciences, Beijing 100101, China; zhaojing1@radi.ac.cn

⁴ College of Land Science and Technology, China Agricultural University, Beijing 100083, China; jxhuang@cau.edu.cn

⁵ Key Laboratory of Remote Sensing for Agri-Hazards, Ministry of Agriculture and Rural Affairs, Beijing 100083, China

⁶ Faculty of Agricultural Engineering, Sindh Agriculture University, Tandojam 70060, Pakistan; msmemon@sau.edu.pk

⁷ College of Engineering, Nanjing Agricultural University, Nanjing 210031, China

⁸ Faculty of Geosciences and Environmental Engineering, Southwest Jiaotong University, Chengdu 610031, China; yingf@swjtu.edu.cn

⁹ CREAf, 08193 Cerdanyola del Vallès, Catalonia, Spain

¹⁰ Department of Global Ecology, Carnegie Institution for Science, Stanford, CA 94305, USA; yzeng@carnegiescience.edu

¹¹ Institute of Remote Sensing Application, Sichuan Academy of Agricultural Sciences, Chengdu 610066, China; keliurs01@gmail.com

* Correspondence: xubaodong@mail.hzau.edu.cn; Tel.: +86-027-8728-5017

Received: 14 February 2020; Accepted: 9 March 2020; Published: 12 March 2020



Abstract: Global biophysical products at decametric resolution derived from Sentinel-2 imagery have emerged as a promising dataset for fine-scale ecosystem modeling and agricultural monitoring. Evaluating uncertainties of different Sentinel-2 biophysical products over various regions and vegetation types is pivotal in the application of land surface models. In this study, we quantified the performance of Sentinel-2-derived Leaf Area Index (LAI), Fraction of Absorbed Photosynthetically Active Radiation (FAPAR), and Fractional Vegetation Cover (FVC) estimates using global ground observations with consistent measurement criteria. Our results show that the accuracy of vegetation and non-vegetated classification based on Sentinel-2 surface reflectance products is greater than 95%, which indicates the vegetation identification is favorable for the practical application of biophysical estimates, as several LAI, FAPAR, and FVC retrievals were derived for non-vegetated pixels. The rate of best retrievals is similar between LAI and FAPAR estimates, both accounting for 87% of all vegetation pixels, while it is almost 100% for FVC estimates. Additionally, the Sentinel-2 FAPAR and FVC estimates agree well with ground-measurements-derived (GMD) reference maps, whereas a large discrepancy is observed for Sentinel-2 LAI estimates by comparing with both GMD effective LAI (LAI_e) and actual LAI (LAI) reference maps. Furthermore, the uncertainties of Sentinel-2 LAI, FAPAR and FVC estimates are 1.09 m²/m², 1.14 m²/m², 0.13 and 0.17 through comparisons to ground LAI_e, LAI, FAPAR, and FVC measurements, respectively. Given the temporal difference between Sentinel-2 observations and ground measurements, Sentinel-2 LAI estimates are more consistent

with LAI_e than LAI values. The robustness of evaluation results can be further improved as long as more multi-temporal ground measurements across different regions are obtained. Overall, this study provides fundamental information about the performance of Sentinel-2 LAI, FAPAR, and FVC estimates, which imbues our confidence in the broad applications of these decametric products.

Keywords: leaf area index (LAI); fraction of absorbed photosynthetically active radiation (FAPAR); fractional vegetation cover (FVC); Sentinel-2; Evaluation; Uncertainty

1. Introduction

The importance of vegetation is widely perceived in studies of land–atmosphere interactions [1–3]. Several biophysical indicators, i.e., Leaf Area Index (LAI), Fraction of Absorbed Photosynthetically Active Radiation (FAPAR), and Fractional Vegetation Cover (FVC), characterize the function of vegetation and are widely used in a broad range of user communities [4–7]. LAI is generally defined as one half of the total green leaf area per unit ground surface area [8]. However, since the mono-angle observation of remote sensing is not sensitive to the possible heterogeneity in leaf distribution within the canopy, LAI derived from the remote sensing is often called effective LAI (hereafter, LAI_e) that assumes a random distribution of leaves in canopy volume [9]. The LAI_e can be converted to the actual LAI (hereafter, LAI) with the associated foliage clumping information as necessary [10]. FAPAR measures the fraction of radiation absorbed by leaves in the 0.4–0.7 μm spectrum [11], and FVC is the ratio of the vertically projected area of vegetation to the total surface area [12]. Due to the high capacities of describing the energy and momentum exchange between the surface and atmosphere, LAI and FAPAR are well-known as essential climate variables (ECVs) by the Global Climate Observing System (GCOS) [13] in terrestrial ecosystems [4,14]. FVC plays a vital role in climatic and hydrologic cycles through plant transpiration, photosynthesis, and surface albedo [12,15,16]. To collect long-term global LAI, FAPAR, and FVC datasets for the monitoring and modeling of large-scale agroecosystems, satellite remote sensing provides an effective way to generate these biophysical products on a regular basis [17].

Several global LAI, FAPAR, and FVC remote sensing products have been generated from different sensors, such as VEGETATION [14,18], MODIS [17,19,20], AVHRR [21–24], VIIRS [25,26], etc. However, most global LAI, FAPAR, and FVC products are available only at hectometer-level (300 m–1000 m) or even coarser spatial resolutions [27,28]. The moderate- or coarse-resolution pixels are usually mixtures of several land cover types due to the heterogeneous land surface, introducing the main errors in the retrieval of biophysical variables [29–31]. For instance, the largest difference between pure and mixed pixels of MODIS LAI products can reach 178% over savanna [32]. Therefore, the finer spatial resolution products of LAI, FAPAR, and FVC are necessary for various applications, especially in regions with heterogeneous landscapes.

In particular, the Sentinel-2 constellation, which comprises Sentinel-2A and Sentinel-2B satellites designed by the European Space Agency (ESA), offers free multi-spectral decametric spatial resolution (10 to 60 m) optical imagery at a 5-day interval over global terrestrial surfaces [33]. Due to its high spatiotemporal resolution observation as well as rich spectral bands, the Sentinel-2 provides an opportunity for opening a new prospect of generating global LAI, FAPAR, and FVC products at decametric spatial resolution. Following the release of Sentinel-2 multi-spectral instrument (MSI) images, the algorithm to derive vegetation biophysical variables (LAI, FAPAR, and FVC) was proposed by Weiss and Baret [34]. Compared to other methods (e.g., look-up table [28], empirical relationship between biophysical variables and vegetation indices [29,35], etc.) to derive biophysical variables, the newly developed algorithm for Sentinel-2 imagery is advantageous in two aspects. First, this algorithm is generic without inputs of the specific land cover type, which can be easily extended for the retrieval of vegetation biophysical variables at the global scale. Second, this algorithm has been

integrated as a Simplified Level 2 Product Prototype Processor (SL2P) tool in the Sentinel Application Platform (SNAP) software (version 7.0.0, <http://step.esa.int/main/download/snap-download/>) and is accessible for public communities to generate biophysical products [36,37]. That is, we can easily use the SL2P tool to derive biophysical estimates at regional to global levels as necessary. Therefore, it can be expected that Sentinel-2 biophysical estimates derived by this algorithm will be broadly used in various fields [37–39]. However, due to the uncertainty associated with data pre-processing and inversion algorithms [40,41], the accuracy of Sentinel-2 LAI, FAPAR, and FVC estimates need to be evaluated for the potential algorithm improvement and wide applications in ecological environment.

The schemes for the evaluation of product performance are generally categorized into two types: direct validation and product intercomparison [42,43]. Direct validation is the most common way to assess products to understand their uncertainties associated with input, pre- or post-processing and inversion algorithms. A lot of previous studies evaluated the product uncertainties by direct validation and offered several ground datasets [40,42]. Although these ground datasets were spatially dispersed, their inadequate spatiotemporal representativeness restricts the evaluation of long-term global products [44,45]. By contrast, product intercomparison mainly evaluates the spatiotemporal coverage and consistency among different products over a long period of time or a large spatial scale, providing additional information on the relative performance of each product [20,42]. Both of these two schemes have been used in the Sentinel-2 derived biophysical estimates [46–48]. For the newly developed S2LP tool in the year 2016 to derive Sentinel-2 LAI, FAPAR, and FVC estimates, several studies [36–39,49–52] reported the uncertainty of these estimates in different regions and observation dates. Nevertheless, previous validation studies suffered from several limitations as follows, which should be addressed for a better understanding on the performances of different biophysical estimates derived from the S2LP tool.

First, the assessment of Sentinel-2 biophysical estimates was generally performed in one or a few regions, and its results were spatially limited [36,49,50]. Second, most validation studies focused on the specific biophysical variable, such as LAI or FAPAR [38,52]. Third, the validation was only implemented on a single vegetation type, i.e., crops or forests [39,49]. Forth, since the retrievals of biophysical variables were evaluated based on the individual field campaigns, the inconsistent measurement criteria may introduce incomparable results for product validation in different studies [37,39,51]. Finally, the sources of uncertainty for deriving these biophysical variables have not been fully explored [38,49]. These knowledge gaps highlight a necessity for a comprehensive evaluation of the Sentinel-2 vegetation biophysical estimates using globally available ground measurements.

This study aims to comprehensively evaluate the Sentinel-2 biophysical estimates over various regions, observation dates and vegetation types using all available in situ data measured in the same criteria and explore the reasons that caused the uncertainty of estimates. Thus, we have generated long-term Sentinel-2 LAI, FAPAR, and FVC estimates to achieve the specific objectives: (i) to evaluate the spatiotemporal coverage of high-quality retrievals for different variables and perform the product intercomparison between Sentinel-2 biophysical estimates and other decametric-resolution reference maps derived by ground measurements over numerous pixels; (ii) to quantify the uncertainty of Sentinel-2 estimates for different vegetation types (i.e., crops, forests, and grasses) using available ground measurements; (iii) to compare the reliability of three Sentinel-2 biophysical estimates, i.e., LAI, FAPAR, and FVC. This paper is organized as follows. Section 2 briefly describes the study area, ground measurements and Sentinel-2 MSI data used in this study. Section 3 introduces the methods for generating Sentinel-2 biophysical estimates and evaluating their performances. Section 4 presents the evaluation results of Sentinel-2 biophysical estimates. Section 5 discusses the possible factors that impact on the accuracy of Sentinel-2 estimates, as well as the limitation of the current study and future directions. Finally, Section 6 provides concluding remarks on this study.

2. Study Area and Data

2.1. Study Area

The study areas were selected based on the ImagineS field campaign (<http://fp7-imagines.eu/pages/services-and-products/ground-data.php>) which aims to validate the satellite-derived biophysical products of the Copernicus Global Land service [53]. ImagineS provides in situ data of 23 sites with the consistent measured criteria during the years 2013–2016. As the first Sentinel-2 satellite was launched on 23 June 2015, 10 sites covering ground measurements over 2015–2016 were further selected for the product validation in this study. The ground measurements marked as yellow dots were mainly located in 5 countries, i.e., Spain, Ukraine, Kenya, France and Italy (Figure 1). Additionally, crops, forests, grasses and bare land were also highlighted in each measurement.

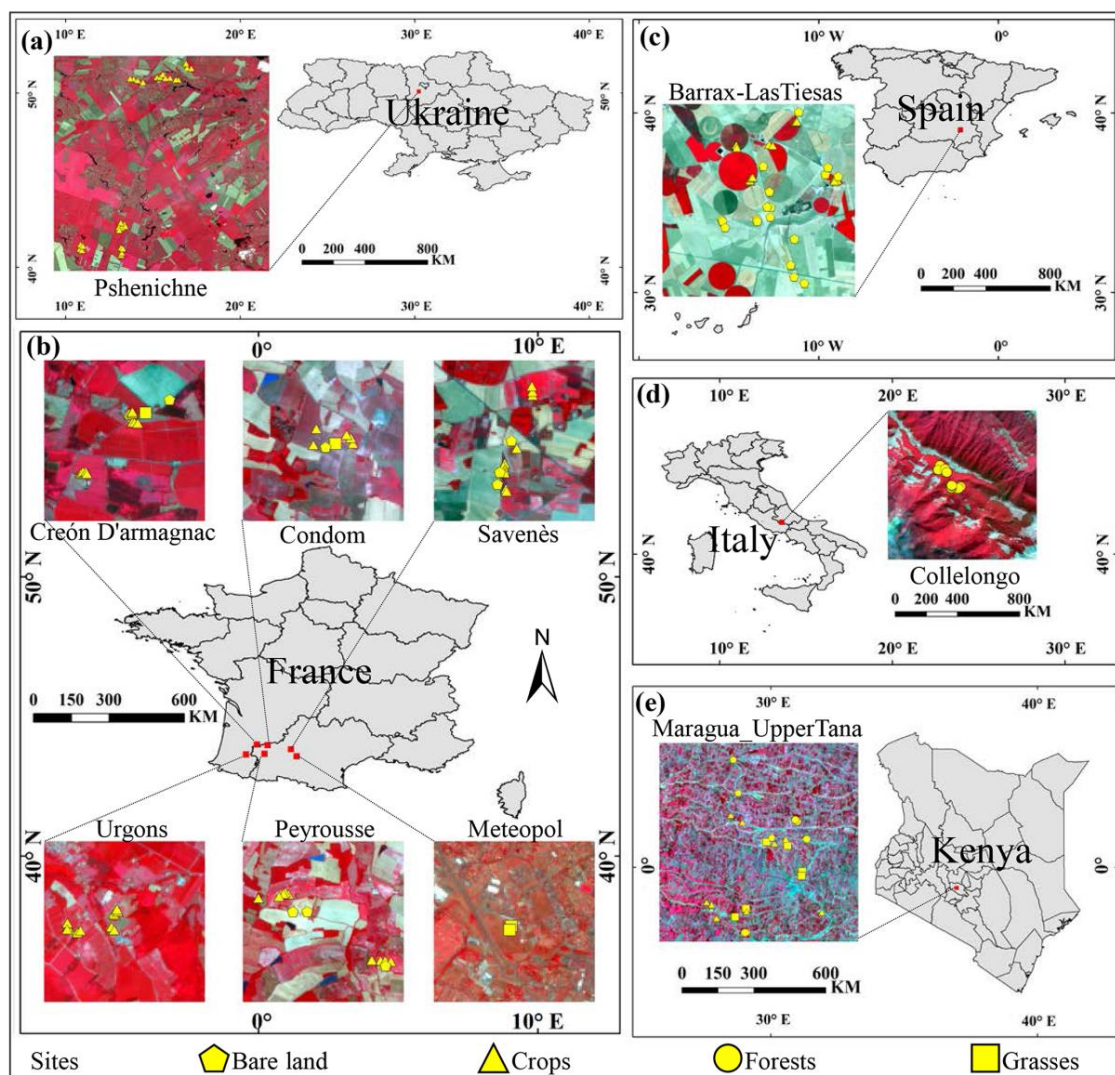


Figure 1. Spatial distribution of the selected sites for which LAI (LAI_e), FAPAR, and FVC measurements were available from 2015 to 2016. The color image (RGB) is a composition of Sentinel-2 three bands, i.e., band 8a (near-infrared), band 4 (red), and band 3 (green), at 20-m spatial resolution, where yellow points represent the ground elementary sampling units (ESUs). (a–e) denote the location of ground measurements in Ukraine, France, Spain, Italy, and Kenya, respectively.

Specifically, the Barrax site in Spain consists of more than 60% dry land and other irrigated land with different crop types, such as corn, wheat, barley, etc. The terrain of this site is flat and its

elevation is around 700 m. The parcel size of cropland is generally over 0.02 km² and this region falls within the cold semi-arid climate based on the Köppen–Geiger climate classification maps [54]. The Pshenichne site in Ukraine is surrounded by winter wheat, maize, soybean, and winter rapeseed in the dry and irrigated land, with the parcel size of approximately 0.01 km², the elevation of 195 m, and the warm-summer humid continental climate. The Maragua_UpperTana site in Kenya is characterized by small parcel size (<0.01 km²) in dry land and a variety of vegetation types, including tea, coffee, banana, etc. The elevation of this site ranges from 1600 to 2000 m, and this site falls within the temperate oceanic climate. The vegetation type of the Collelongo site in Italy is dominated by the deciduous forest, i.e., European beech. This region is located in the warm-summer humid continental climate and its elevation is from 700 to 1900 m. The other 6 sites in France are generally flat (elevation: 100–300 m) with large crop types in both the irrigated land (maize and soybean) and dry land (sunflower, wheat and rapeseed), and only the Meteopole site and Condom site have some grasses and deciduous forests, respectively. The parcel size of cropland changes from less than 0.01 km² to more than 0.05 km², and all sites are grouped into the temperate oceanic climate.

2.2. Ground Truth Data and Ground-measurements-derived (GMD) Reference Maps

For each study area, more than ten elementary sampling units (ESUs) were selected, and the area of each ESU was 20 m × 20 m, which is identical to the spatial resolution of Sentinel-2 biophysical estimates. The 10–25 sampling plots were measured using different sampling schemes for various types of plantations (e.g., the three sampling schemes for random, row or tree plantation were shown in Figure A1 in Appendix A) in each ESU, and the spatial location of each ESU was recorded using a global positioning system (GPS) [55,56]. Then, all measured variables in this ESU were averaged to represent the corresponding value of the whole ESU. Several instruments, including the LAI-2200 plant canopy analyzer, AccuPAR ceptometer and Digital Hemispherical Photography (DHP), were used to measure LAI_e, LAI, FAPAR, and FVC, respectively, at these sites. The LAI-2200 and AccuPAR can only generate LAI_e due to the randomness assumption of leaf distribution on canopy architecture in these instruments [57]. The LAI can be calculated from DHP because it can derive LAI_e and clumping index simultaneously. Since the algorithm of the Sentinel-2 LAI estimate did not involve the clump index, it can only derive the LAI_e retrievals. Thus, to better understand the performance of the LAI algorithm and LAI estimates in practice, both LAI_e and LAI ESUs were used in this study. The FAPAR and FVC can be also estimated from DHP. Specifically, the gap fraction was first derived from the DHP images with the classification of vegetation and background elements, and then both FAPAR and FVC were calculated based on the derived gap fraction [58]. More details about the measured ESUs at each site are depicted in Table 1 in Section 2.3. Moreover, the number of ESUs is different for the 4 variables (LAI_e, LAI, FAPAR, and FVC) because they were measured by different instruments (DHP, LAI-2200, and AccuPAR) at several sites. It should be noted that the variable of harvested crops or bare land was also included in ground ESUs, introducing larger standard deviation of measured biophysical variables at several sites, such as Barrax, Peyrousse, Savenès, etc.

The GMD reference maps with 30-m spatial resolution, which are useful to assess the quality of kilometeric biophysical products, were derived using these ground ESUs and were provided by the ImagineS field campaigns [53]. Specifically, a transfer function, which employed a multivariate ordinary least squares regression with an iteratively re-weighted least squares method, was established based on the ground ESUs and the reflectances from Landsat-8 Operational Land Imager (OLI) scenes [55]. Then, this empirical relationship was employed to generate the reference maps for the whole study area. Since the GMD reference maps were widely used as the benchmark data for the land surface models and the validation of coarse resolution products, the intercomparison with GMD reference maps can assess the potential Sentinel-2 biophysical estimates for different applications.

Table 1. The acquisition dates (Year-DOY (Day of Year)) of in situ measurements and Sentinel-2A images. The number, average (μ) and standard deviation (σ) of ground ESUs are reported in the last 4 columns. The “-” indicates that no available satellite data at this site.

Site Name	Country	Year-DOY		Ground ESU Number ($\mu \pm \sigma$)			
		In-situ Measurements	Sentinel-2A (cloud free)	LAI _e (m ² /m ²)	LAI (m ² /m ²)	FAPAR	FVC
Barrax	Spain	2015-203	2015-207	44 (1.58 ± 1.61)	35 (1.67 ± 2.04)	35 (0.37 ± 0.42)	35 (0.34 ± 0.39)
Pshenichne	Ukraine	2015-188	2015-197	28 (2.14 ± 0.36)	28 (3.28 ± 0.95)	28 (0.81 ± 0.04)	28 (0.70 ± 0.08)
		2015-204	2015-214	28 (2.56 ± 0.36)	28 (3.78 ± 0.79)	28 (0.85 ± 0.05)	28 (0.73 ± 0.12)
Meteopol	France	2015-173	2015-187	2 (0.52 ± 0.06)	2 (0.55 ± 0.08)	2 (0.34 ± 0.02)	2 (0.35 ± 0.05)
Peyrousse		2015-174	2015-187	12 (0.51 ± 0.44)	12 (0.89 ± 0.78)	12 (0.32 ± 0.24)	12 (0.33 ± 0.25)
Urgons		2015-174	2015-187	12 (0.92 ± 0.25)	7 (1.67 ± 0.50)	7 (0.47 ± 0.12)	7 (0.39 ± 0.08)
Creón D’armagnac		2015-175	2015-187	14 (2.40 ± 1.23)	8 (3.05 ± 1.94)	9 (0.61 ± 0.34)	8 (0.49 ± 0.31)
Condom		2015-176	2015-187	8 (0.77 ± 0.42)	8 (1.24 ± 0.76)	8 (0.43 ± 0.22)	8 (0.42 ± 0.22)
Savenès		2015-176	2015-187	13 (0.74 ± 0.57)	10 (0.77 ± 0.69)	10 (0.32 ± 0.29)	10 (0.31 ± 0.27)
Collelongo	Italy	2015-189	-	15 (2.63 ± 0.32)	15 (3.62 ± 0.56)	15 (0.83 ± 0.04)	15 (0.78 ± 0.06)
		2015-268	2015-262	15 (2.78 ± 0.22)	15 (3.79 ± 0.35)	15 (0.86 ± 0.17)	15 (0.86 ± 0.03)
Maragua_UpperTana	Kenya	2016-068	2016-075	26 (1.33 ± 1.31)	26 (1.78 ± 1.38)	26 (0.55 ± 0.32)	26 (0.54 ± 0.32)

2.3. Sentinel-2 MSI Data

The Sentinel-2A and Sentinel-2B satellites were launched on 23 June 2015 and 7 March 2017, respectively. Both of them have very similar MSI band characteristics and the same spatiotemporal resolution. The combination of two satellites can provide a revisit cycle of better than 5 days for observations globally. The MSI bands cover the visible, near-infrared, and shortwave-infrared spectral domains. According to the band information of Sentinel-2 MSI, the spatial resolution, central wavelength, band width and normalized spectral response of each band were displayed, and the bands used to derive the biophysical variables are highlighted in Figure 2.

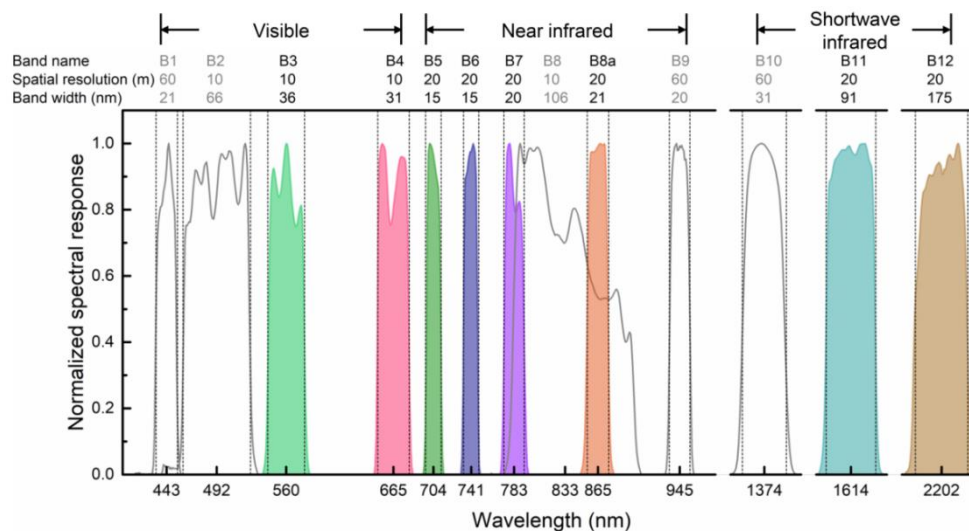


Figure 2. The normalized spectral response of Sentinel-2A multi-spectral instrument (MSI) bands. These bands cover the visible, near-infrared, and shortwave-infrared spectral domains. The top three rows show the name, spatial resolution, and width of each band, respectively. The filled area indicates the selected bands (bands 3–7, 8a, and 11–12) for the LAI, FAPAR, and FVC retrievals.

According to the spatial location and acquisition date of ground ESUs, the corresponding Sentinel-2 MSI data were downloaded from the ESA Copernicus Open Access Hub (<https://scihub.copernicus.eu/dhus/#/home>). Due to the limited temporal coverage (2015–2016) of ground ESUs, only Sentinel-2A data can be used in this study. Table 1 shows the observation dates of ground ESUs and Sentinel-2A MSI data, as well as the number of ground ESUs for LAI_e, LAI, FAPAR,

and FVC at each site. We carefully selected Sentinel-2 data by considering the criteria of no cloud contaminations and the minimal gap of observation dates between ground ESUs and Sentinel-2A data. As a result, seven tiles, i.e., T30TYP, T31TCJ, T35UQR (2 dates), T30SWJ, T33TUG, and T37MBV, were acquired for ten sites. For these sites, the dates of several Sentinel-2A images were not exactly consistent with those of ground ESUs. This is primarily due to the relatively long revisit cycle (10 days) of a single Sentinel-2 satellite, as well as cloud effects. Hence, the impact of the temporal gap between ground measurements and Sentinel-based products needs to be further considered in the validation result. The Level-1C products of Sentinel-2A, which have already been corrected for radiometric and geometric uncertainties, were downloaded for each site. Since the Level-1C product only provides the top of atmosphere (TOA) reflectance, we used the Sen2Cor processor (version 2.5.5, http://step.esa.int/main/third-party-plugins-2/sen2cor/sen2cor_v2-5-5/) to generate atmospherically corrected surface reflectance (Level-2A) from Level-1C products. Additionally, the result of the Sen2Cor processor can provide the scene classification layer including the detection of atmospheric influences (cloud, cloud shadow, cirrus, etc.) and land cover types (vegetation, not-vegetated and water). The pixel accuracy of cloud identification was approximate 90% according to the previous study [59], and this layer has been widely used to select the high-quality vegetation pixels in validation activities of Sentinel-2 biophysical estimates [37,38,49]. Moreover, the accuracy of vegetation and non-vegetated identifications from this layer will be further evaluated in Section 4.1 to indicate the reliability of this layer in the validation of Sentinel-2 biophysical estimates. Due to the different spatial resolutions (10- and 20-m) for band 3–7, 8a, and 11–12, the reflectances of these bands were resampled to the 20-m grid to match the ground ESU using the nearest neighbor method integrated in the Sentinel Application Platform (SNAP).

3. Methodology

3.1. Generation of Sentinel-2 LAI, FAPAR, and FVC Estimates

The theoretical algorithms of LAI, FAPAR, and FVC retrievals were developed based on the neural network [34]. Specifically, the process of this algorithm includes three main steps: generating the training datasets through the PROSAIL model, calibrating the neural network and predicting biophysical variables using the trained neural network, as shown in Figure 3. The PROSAIL model [60] couples the Scattering from Arbitrarily Inclined Leaves (SAIL) canopy bidirectional reflectance model [61] and the PROSPECT leaf optical properties model [62], which were used to describe the influence of canopy structure and leaf property on the canopy reflectance, respectively. The value distribution patterns for the input variables of the PROSPECT model were determined by the prior knowledge from the literature data as well as the individual vegetation type. For the input variables of the SAIL model, the soil reflectance was mainly derived from a soil reflectance database representing a large variation of soil characteristics [63,64]. The LAI and average leaf angle (ALA) distributions were established from the VALERI dataset, while the valid range of hot spot parameter (h_{spot}) was derived from a previous study [65]. The directional information, including solar zenith angle, view zenith angle and relative azimuth angle between solar and view acquired from Sentinel-2 images, was taken into account in the PROSAIL model to simulate the corresponding canopy reflectance. More details about the distribution of input variables were described in Weiss and Baret [34].

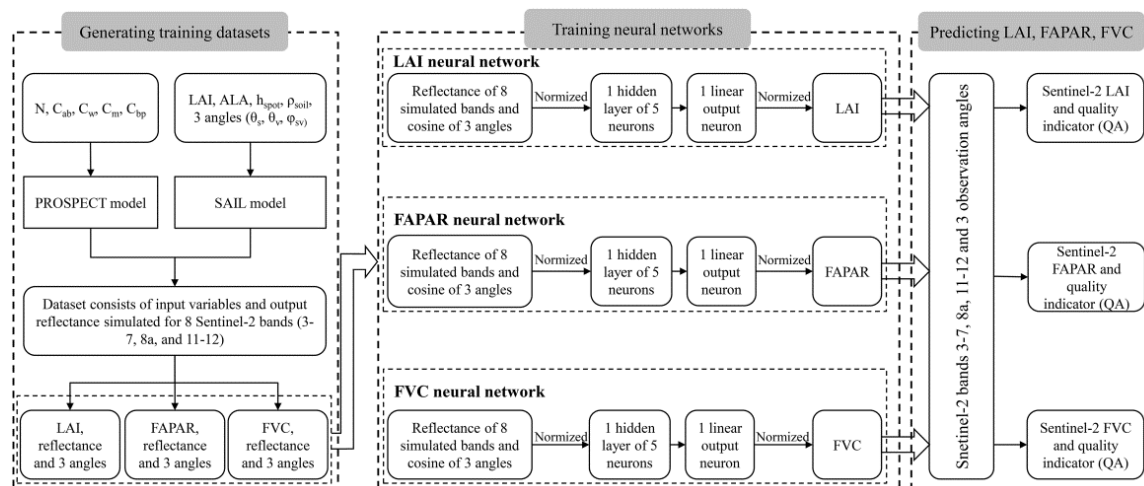


Figure 3. The framework of the Leaf Area Index (LAI), Fraction of Absorbed Photosynthetically Active Radiation (FAPAR), and Fractional Vegetation Cover (FVC) retrieval algorithm for Sentinel-2 imagery. The “N”, “ C_{ab} ”, “ C_w ”, “ C_m ”, “ C_{bp} ” in the PROSPECT model and “LAI”, “ALA”, “ h_{spot} ”, “ ρ_{soil} ”, “ θ_s ”, “ θ_v ”, “ φ_{sv} ” in the Scattering from Arbitrarily Inclined Leaves (SAIL) model denote mesophyll structure index, chlorophyll content ($\mu\text{g}/\text{cm}^2$), dry matter content (g/cm^2), water content (g/cm^2), brown pigment content for leaf and leaf area index (m^2/m^2), average leaf angle ($^\circ$), hot spot parameter, soil reflectance, solar zenith angle ($^\circ$), view zenith angle ($^\circ$), relative azimuth angle between solar and view ($^\circ$), respectively.

The derived dataset from the PROSAIL model was then used for training the neural network. Eight bands from the Sentinel-2 MSI in Section 2.3 were used to retrieve biophysical variables, given that other bands are more sensitive to atmosphere or clouds. Note that the generated canopy reflectance was simulated to fit the Sentinel-2 bands by considering the noises embedded in different wavebands. The neural network consisted of 3 layers: the input layer, hidden layer and output layer. The input layer includes 11 neurons, which represented 11 input variables: canopy reflectance of 8 spectral bands and the cosine of 3 angles that refer to the geometry of observation (solar zenith angle, view zenith angle and relative azimuth angle between solar and view). The hidden layer contains 5 neurons with tangent sigmoid transfer functions. Since a single variable was derived from the output layer with a separate linear transfer function, a total of 3 neural networks were needed for respectively generating LAI, FAPAR, and FVC retrievals. As the biophysical algorithm has been integrated as a S2LP tool in SNAP, this S2LP tool was applied to the Sentinel-2 surface reflectance to generate LAI, FAPAR, and FVC estimates for all decametric resolution pixels. Each biophysical estimate also contains the corresponding quality indicators (QA) that enables us to better understand the spatial structure of uncertainties. The key indicator to characterize the quality of estimates is the valid range of input and output variables, which can be grouped into the following 3 categories: (1) the best retrievals ($QA = 0$); (2) the input out of range ($QA = 1$); (3) the output out of range ($QA > 1$).

3.2. Evaluation of Estimate Quality and Comparison with GMD Reference Maps

The qualities of Sentinel-2 LAI, FAPAR, and FVC estimates were first evaluated in this study, including the classification accuracy of vegetation and non-vegetated pixels and the spatial coverage of best retrievals. Note that the evaluation processes were implemented using the quality control layer to exclude pixels that were contaminated by clouds, cloud shadow, cirrus and snow. First, the classification accuracy of vegetation and non-vegetated pixels needs to be evaluated because the algorithm derived biophysical variables without the inputs of the specific land cover types. Although the algorithm introduced the reflectance spectra representing a large variation of soil types and provided the QA layer with the input out of range ($QA = 1$) to reduce the impacts of non-vegetated

pixels, many vegetation pixels without cloud contaminations were also identified as this case based on visual inspection. Similarly, the abnormal situation that a lot of non-vegetated pixels were labeled as the best retrieval (QA = 0) was observed due to the imperfect algorithm. That is, the LAI, FAPAR, and FVC retrievals derived from the algorithm may be greater than 0 for non-vegetated pixels. This result likely introduces undesired errors in the application of Sentinel-2 estimates. Thus, the layer of vegetation and non-vegetated classification is essential to utilize these estimates properly, and its accuracy should be evaluated.

Second, as a vital indicator of the quality of retrievals, the algorithm path of each pixel is stored in the QA layer of each Sentinel-2 biophysical estimate. By comparing the retrieval rate of different algorithm paths, we can evaluate the overall quality of the biophysical estimate. Moreover, an indicator called the retrieval index (RI) that characterizes the proportion of the high-quality retrievals [25,66] was adopted to show the spatial coverage of the best retrievals with no cloud, cloud shadow, cirrus and snow contaminations. The RI of each Sentinel-2 tile selected in this study was calculated using Equation (1).

$$RI = \frac{\text{Number of the best retrieved pixels}}{\text{Number of total vegetation and cloud - free pixels}} \times 100\% \quad (1)$$

Third, the performance of Sentinel-2 time-series biophysical estimates was analyzed over three sites representing three vegetation types (crops, forests, and grasses). Since the first Sentinel-2 satellite was launched on 23 June 2015, all Sentinel-2 images from July 2015 to July 2018 were acquired over three tiles, i.e., T35UQR, T33TUG, and T37MBV. To reduce the undesired variability caused by cloud/cloud shadow/cirrus/snow/ice contaminations, only high-quality observations (pixels were labeled as vegetation or non-vegetated) were further selected based on the scene classification layer from the surface reflectance products. The QA values of each biophysical variable were also extracted to show their evolutions across seasonal and annual contexts. Moreover, the corresponding ground ESUs at each selected site were added to evaluate the accuracy of Sentinel-2 biophysical estimates.

Finally, the high-resolution GMD reference maps are generally served as benchmarks for the assessment of kilometric satellite-derived biophysical products or inputs for land surface models at the regional level [4,43]. The evaluation of the spatial consistency between Sentinel-2 estimates and GMD reference maps was thus essential to analyze the potential of Sentinel-2 estimates in various applications. To spatially match Landsat-based GMD reference maps and Sentinel-2 derived retrievals, the Sentinel-2 estimate was projected to the same coordinate system as the GMD reference map and was resampled to the 30-m grid using the nearest neighbor method. Several statistical metrics (Bias, root mean square error (RMSE), and coefficient of determination (R^2)) were adopted for the analysis of each Sentinel-2 derived biophysical estimate.

3.3. Uncertainty Quantification

The uncertainty is characterized using the RMSE between Sentinel-2 biophysical estimates and the corresponding benchmark values. In this study, the ground ESUs were employed as the benchmark to quantitatively analyze the uncertainty of the Sentinel-2 biophysical estimates. Based on the available ground ESUs (Table 1), we carefully selected the valid pixel of Sentinel-2 estimates following three criteria: (i) the vegetation pixel; (ii) the pixel with no cloud, cloud shadow, cirrus and snow contaminations; (iii) the best retrieval from the neural network algorithm. As a result, a total of 111 LAI_e, 97 LAI, 98 FAPAR, and 128 FVC ground ESUs were used in this study. Additionally, the GCOS identified target requirement uncertainties of max (0.5, 20%) for LAI product and max (0.05, 10%) for FAPAR product [13], which was also taken as the criteria to evaluate the corresponding Sentinel-2 biophysical estimates. Finally, the performance of Sentinel-2 biophysical estimates was also analyzed for individual vegetation types, i.e., crop types, forests, and grasses.

4. Results

4.1. The Accuracy of Vegetation and Non-vegetated Pixel Classification

According to the scene classification algorithm described in Sentinel-2 surface reflectance products algorithm theoretical basis document (ATBD), the vegetation or non-vegetated pixels were identified using NDVI and a reflectance ratio index defined by the ratio of the reflectance of the near-infrared band to that of the green band. Since the latter index was built for monitoring the senescing vegetation, NDVI, which is advantageous to distinguish the growing vegetation and other types, was used in this study. We calculated the histogram of NDVI from all selected tiles, i.e., seven tiles in Section 2.3, for vegetation and non-vegetated pixels, as shown in Figure 4. Among tens of millions of pixels without cloud contaminations, the mean NDVIs of vegetation and non-vegetated pixels were 0.71 and 0.28, respectively, which were calculated from all vegetation (red area in Figure 4) and non-vegetated (blue area) pixels. Although the mean NDVIs of different land cover types were quite different, Figure 4 shows their NDVIs had some overlaps, from 0.40 to 0.60. It is noteworthy that the uncertainty of non-vegetated pixel classification cannot be neglected, as a pixel is likely covered by vegetation when its NDVI is greater than 0.40, based on previous in situ measurements [67–70]. Therefore, the NDVI overlap between vegetation and non-vegetated pixels, as well as the uncertainty of non-vegetated pixel classification, are potentially key factors that affect the accuracy of vegetation and non-vegetated pixel identification in the scene classification layer from Sentinel-2 surface reflectance products.

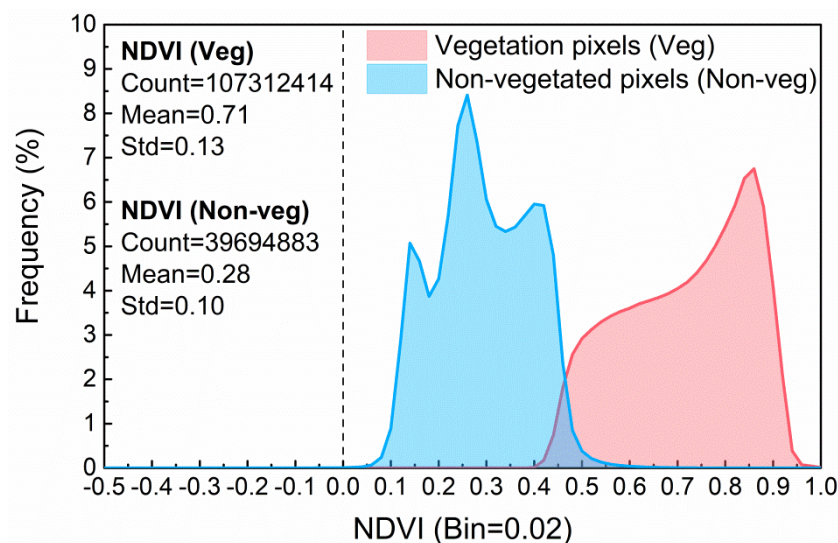


Figure 4. The histogram of NDVI for vegetation (red area) and non-vegetated (blue area) pixels, respectively. The statistical results (pixel count, mean and standard deviation (std) value of pixels) for all vegetation (red area) and non-vegetated (blue area) pixels are shown in the left panel.

According to the spatial distribution of ground ESUs, a total of 202 pixels were selected from the scene classification layer and the evaluation results are shown in Table 2. Among these pixels, the number of unclassified pixels (=1) can be negligible. Note that the cloud-contaminated pixels were excluded to achieve a reliable result. Among the 183 valid pixels, six vegetation pixels were identified as non-vegetated pixels in the Sentinel-2 scene classification layers. We checked the NDVI of these six pixels and found that their values ranged from 0.38 to 0.47, which confirms our aforementioned analysis that the NDVI overlap (Figure 4) between vegetation and non-vegetated pixels is one of the possible causes for the vegetation misclassification. Overall, the accuracy of vegetation and non-vegetated classifications were 96.13% and 100%, respectively, indicating the vegetation or non-vegetated pixel identifications agree well with ground investigations by integrating NDVI

information. Therefore, the scene classification layer is valuable to identify the vegetation pixels in the Sentinel-2 biophysical estimates.

Table 2. The evaluation results of vegetation and non-vegetated pixel identifications in the scene classification layer from Sentinel-2 surface reflectance products based on the investigations of ground ESUs.

Sentinel-2 Scene Classification Layer						
Ground ESUs	Unclassified	Cloud	Land cover	Vegetation	Non-vegetated	Accuracy
	1	18	Vegetation	149	6	96.13%
			Non-vegetated	0	28	100%

4.2. Spatial Coverage of Biophysical Retrievals from Different Algorithm Paths

As indicated in Section 4.1, the pixel identified as vegetation in the scene classification layer was selected at each site because this pixel was not contaminated by cloud, cloud shadow, cirrus, and snow. The number of these high-quality pixels was calculated by each whole tile of Sentinel-2, as shown in Figure 5a. Since not all Sentinel-2 images have full observations in the whole tile, the number of high-quality pixels for several sites (Barrax, and Pshenchine (2015-188)) was less than for other sites. However, we can observe that millions of vegetation pixels were available for each site, indicating the reliability of the RI evaluation results. The proportion of pixels from different algorithm paths exhibited a large discrepancy for LAI, FAPAR, and FVC estimates (Figure 5b–d). For LAI retrievals (Figure 5b), the RI was greater than 75% at each tile and 87.3% for overall tiles. The other poor-quality retrievals, accounting for 12.4% of all vegetation pixels, were mainly caused by the input being out of range. The reasons for the input being out of range in the trained neural networks are likely from three aspects: (i) the imperfection of the RTM model, i.e., PROSAIL, in simulating canopy reflectance; (ii) the range of input variables, such as Cab, ALA, LAI, etc., cannot represent all actual cases; (iii) uncertainties in atmospheric correction for Sentinel-2A MSI images. The former two cases inevitably introduce errors in the generation of training datasets, while the last case refers to the errors embedded in the input surface reflectance.

For FAPAR estimates (Figure 5c), the overall distribution of retrievals from different algorithm paths was quite similar to that of LAI estimates. Nevertheless, two sites, i.e., Barrax and Pshenchine (2015-188), exhibited the proportion of retrievals caused by the output being out of range was about 5%. Therefore, the out of range issue of FAPAR retrievals needs to be further considered in the algorithm improvement and the applications of this product. By contrast, the highest RI (almost 100%) for FVC estimates (Figure 5d) over each site indicated the robustness of the retrieval algorithm. The observed RI differences for LAI, FAPAR, and FVC estimates emphasize that assessing the spatial coverage of high-quality retrievals should be a pre-requisite to more comprehensively understand the performance of different Sentinel-2 biophysical estimates.

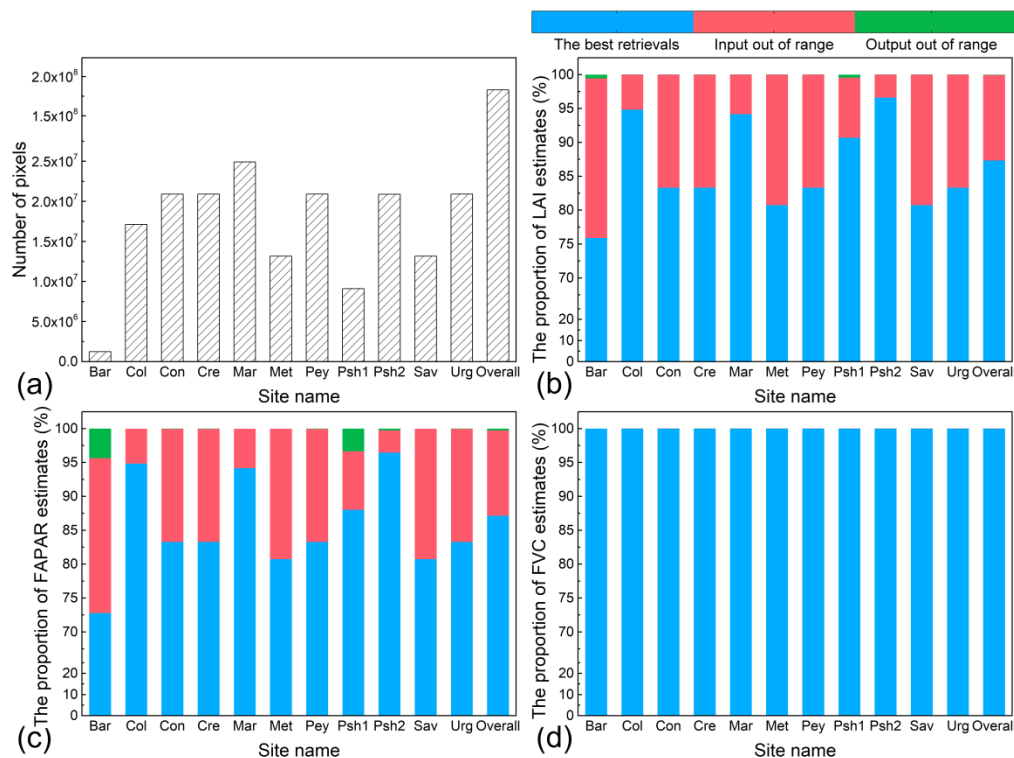


Figure 5. (a) The number of pixels used in evaluating the spatial coverage of retrievals from different algorithm paths for Sentinel-2 biophysical estimates at each site. The pixel identified as vegetation in the scene classification layer was selected. The proportion of (b) LAI, (c) FAPAR, and (d) FVC estimates with the best retrievals, input out of range, and output out of range in all vegetation pixels at each site was also displayed. The “Bar”, “Col”, “Con”, “Cre”, “Mar”, “Pey”, “Psh1”, “Psh2”, “Sav”, and “Urg” are the abbreviation name of Barrax, Collelongo, Creón D’armagnac, Maragua_UpperTana, Peyrouse, Pshenichne (2015-188), Pshenichne (2015-204), Savenès, and Urgons sites.

4.3. Analysis of Sentinel-2 Time-Series Biophysical Estimates

Figure 6 shows the seasonal trajectory of Sentinel-2 biophysical estimates as well as their QA values and the ground ESUs over three example sites (crops, forests, and grasses) for three years (July 2015–July 2018). Overall, the number of valid observations increased from the year 2017 for all sites, which is primarily due to the additional inclusion of Sentinel-2B data. For the crop site (50.001°N , 30.142°E), Sentinel-2 biophysical estimates displayed the typical seasonality of crop growth (Figure 6a), with higher values for dates with obvious vegetation than those dates without vegetation. The LAI, FAPAR, and FVC showed the similar seasonal trajectory because of the highly physical correlations among them. However, only the QA values of LAI and FAPAR estimates were similar, which were quite different from those of the FVC estimates. For the inferior quality of LAI and FAPAR estimates at different observation dates, the outputs out of range ($\text{QA} > 1$) of almost all estimates were caused by the non-vegetated observations, while the estimates with inputs out of range ($\text{QA} = 1$) were observed at both non-vegetated and vegetation observations.

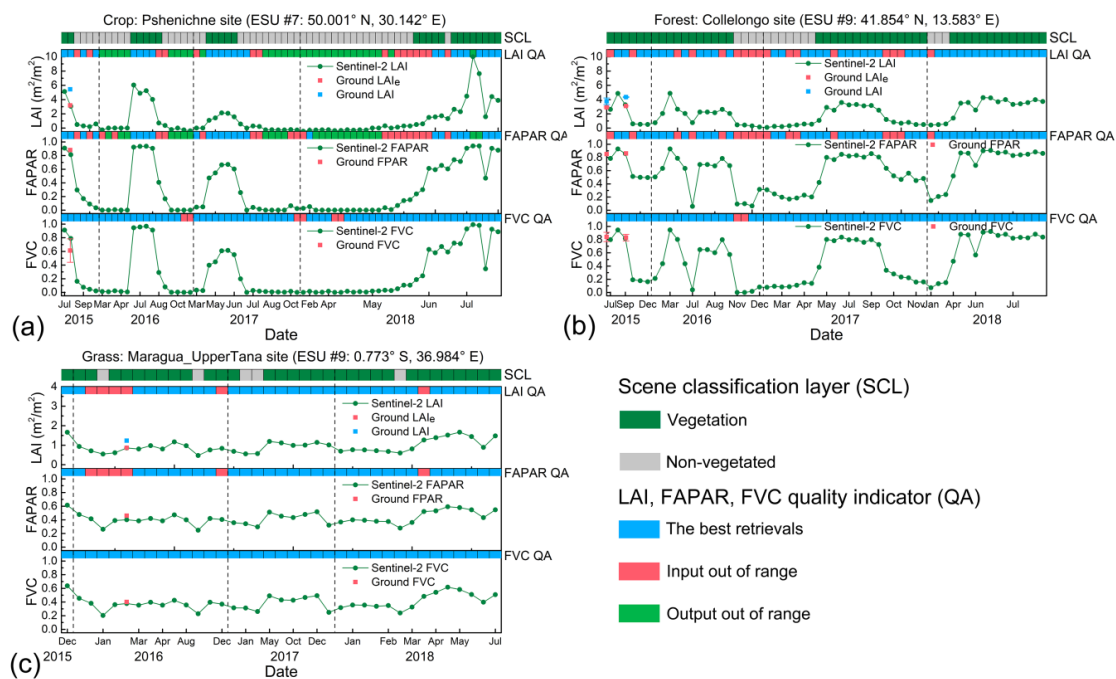


Figure 6. The temporal trajectory of Sentinel-2 LAI, FAPAR, and FVC estimates from July 2015 to July 2018 at the (a) crop site, (b) forest site, and (c) grass site, respectively. The square point indicates the value of the ground ESU. The scene classification layer (SCL) shown at the top of each panel was extracted from Sentinel-2 surface reflectance products. The quality indicator (QA) was also displayed together with the biophysical variable for each observation date.

For the forest site (41.854°N, 13.583°E), all Sentinel-2 biophysical estimates displayed the distinct seasonality of a mid-latitude temperate forest (Figure 6b). The abnormal estimates were found in July 2016, which may be the consequences of unfavorable atmospheric conditions, such as the residual cloud effects that caused the input to be out of range. For the grass site (0.773°S, 36.984°E), the number of valid observations was much less than that of crop and forest sites due to the higher cloudiness at the equatorial region. Thus, Sentinel-2 cannot track the seasonal variation of LAI, FAPAR, and FVC estimates because of the insufficient time-series observations. Indeed, although Sentinel-2 comprises two satellites, which can be combined to improve the temporal continuity of biophysical estimates, it can be observed that several key stages of vegetation were lacking. However, the agreements with the ground LAI_e, FAPAR, and FVC ESUs at each site indicate the good performance of Sentinel-2 time-series biophysical estimates.

4.4. Intercomparison with GMD LAI, FAPAR, and FVC Reference Maps

The Sentinel-2 LAI, FAPAR, and FVC estimates were further compared with overall vegetation pixels of GMD reference maps. Similarly, the vegetation pixels were identified by the scene classification layer from Sentinel-2 surface reflectance products. Figure 7 illustrates the density scatter plots for LAI_e, LAI, FAPAR, and FVC comparisons between Sentinel-2 estimates and GMD reference maps. It was observed that Sentinel-2 LAI estimates showed a slight overestimation (Bias = 0.26 m²/m²) across the whole range of LAI_e values (Figure 7a). In particular, the higher LAI values (> 4 m²/m²) of Sentinel-2 estimates departed from those of GMD LAI_e reference maps, introducing a large positive bias. This difference can be attributed to the high sensitivity of red-edge bands to high LAI values [71–73]. Since the GMD LAI_e maps were derived from Landsat-8 data without red-edge bands, the saturation of reflectance results in lower LAI_e values. For the LAI comparison shown in Figure 7b, Sentinel-2 LAI estimates exhibited some underestimations (Bias = −0.42 m²/m²) compared with GMD LAI reference maps because the LAI is greater than LAI_e based on ground measurements. Overall, Sentinel-2

LAI estimates were more consistent with GMD LAI_e reference maps (RMSE = 0.89 m²/m²) than LAI reference maps (RMSE = 1.04 m²/m²). This is not surprising since the algorithm of Sentinel-2 LAI estimate did not consider the clumping effect and consequently the LAI retrievals should be more consistent with LAI_e. In terms of FAPAR comparison (Figure 7c), the agreement of Sentinel-2 estimates with GMD reference maps was quite good, with small bias (Bias = −0.06) and low uncertainty (RMSE = 0.15). Additionally, no significant bias (Bias = −0.05) was observed for FVC comparison between Sentinel-2 estimates and GMD reference maps (Figure 7d). The performance of Sentinel-2 FVC estimates was similar to that of Sentinel-2 FAPAR estimates when compared to the GMD reference maps. Nevertheless, both Sentinel-2 FAPAR and FVC estimates were lower than the GMD reference maps for the large values (> 0.8).

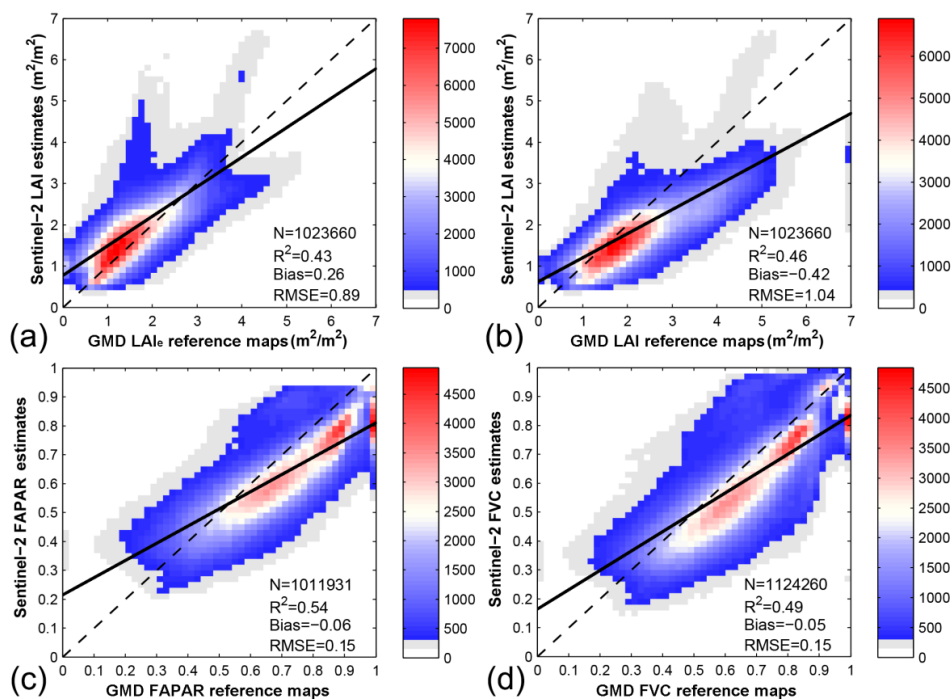


Figure 7. The biophysical-specific comparison between ground-measurements-derived (GMD) reference maps and Sentinel-2 estimates at the pixel scale from 2015 to 2016. The solid black and dash black lines represent the linear fit for all pixels and 1:1 line, respectively. The colorbar shows the density of pixels falling at each grid. (a)–(d) stand for LAI_e, LAI, FAPAR, and FVC comparison, respectively.

4.5. Uncertainty Assessment

Figure 8 shows the uncertainty of Sentinel-2 biophysical estimates that were evaluated by the collected ground ESUs. The performance of Sentinel-2 estimates differed with biophysical variables. The best agreement with ground ESUs was observed for FAPAR estimates, whereas LAI estimates performed at an inferior level when compared to both the ground LAI_e and LAI ESUs. The performance of FVC estimates with the corresponding ground ESUs was also good, with almost no bias and low uncertainty, although some variations were observed for low FVC values. Overall, although Sentinel-2 LAI estimate represents the LAI_e according to the developed algorithm, Figure 8a,b show some overestimations (Bias = 0.57 m²/m²) and underestimations (Bias = −0.40 m²/m²) by the confrontation with ground LAI_e and LAI ESUs, respectively. Furthermore, Sentinel-2 LAI estimates exhibited better agreement with ground LAI_e ESUs ($R^2 = 0.42$) than LAI ESUs ($R^2 = 0.39$), with lower RMSE. The proportion of Sentinel-2 LAI pixels satisfying the GCOS uncertainty requirement (max (0.5, 20%)) was 46.85% and 40.21% for representing LAI_e and LAI, respectively. It should be noted that Sentinel-2 LAI showed the considerable overestimation for the medium LAI (1.5 m²/m² < LAI < 3.5 m²/m²) compared

with ground LAI_e ESUs, whereas the dispersion of Sentinel-2 LAI estimates with ground LAI ESUs was larger than that with ground LAI_e ESUs.

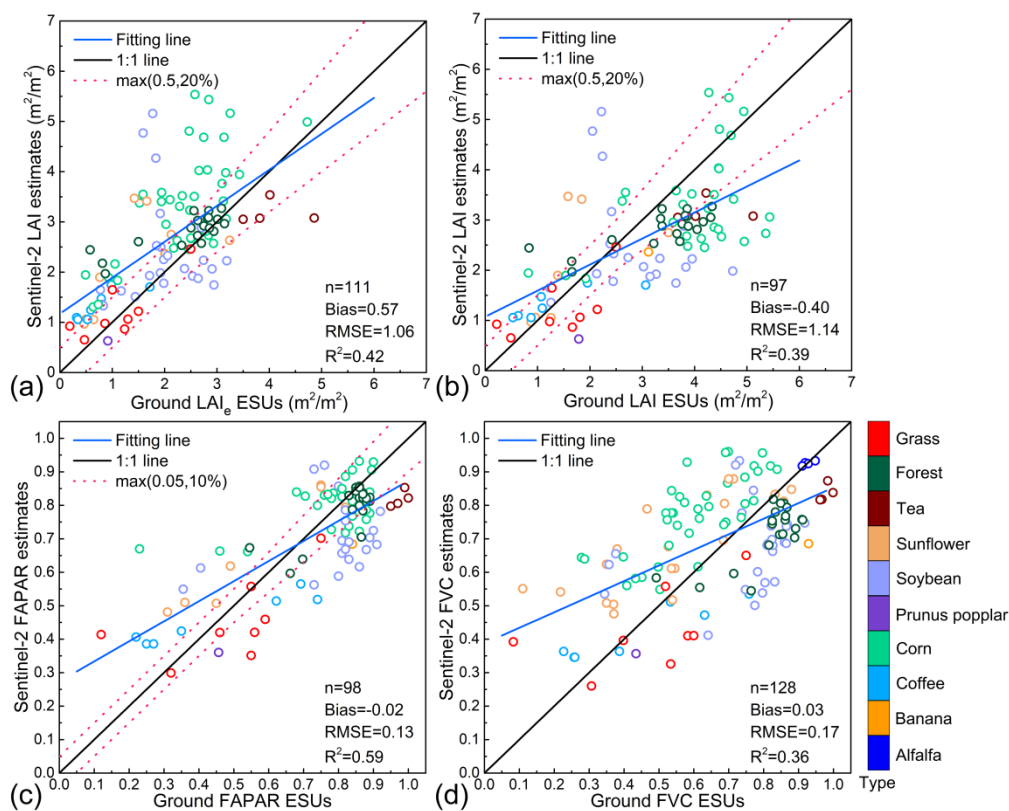


Figure 8. The comparisons between ground ESUs and Sentinel-2 biophysical estimates. (a) Ground LAI_e ESUs versus Sentinel-2 LAI estimates; (b) Ground LAI ESUs versus Sentinel-2 LAI estimates; (c) Ground FAPAR ESUs versus Sentinel-2 FAPAR estimates; (d) Ground FVC ESUs versus Sentinel-2 FVC estimates. The colors stand for different vegetation types (i.e., crop types, forests, and grasses, respectively) shown in the right colorbar. The blue and black solid lines denote the fitting line and 1:1 line, respectively. The red dashed lines show the Global Climate Observing System (GCOS) specifications boundaries for LAI_e (max (0.5, 20%), LAI (max (0.5, 20%)) and FAPAR (max (0.05, 10%)).

For FAPAR, the values of most pixels were distributed between 0.7 and 1.0, but the bias and RMSE were only -0.02 and 0.13 , respectively, indicating the good performance of Sentinel-2 FAPAR estimates. Nevertheless, the dispersion of Sentinel-2 FAPAR cannot be ignored as the R^2 was relatively low ($=0.59$). Moreover, Sentinel-2 FAPAR estimates that meet the uncertainty requirements (max (0.05, 10%)) suggested by GCOS accounted for 45.92% among 98 ground ESUs. For FVC, the number of pixels ($n = 128$) used for the validation was much larger than that for LAI and FAPAR because of its good spatial coverage (Figure 5d). The Sentinel-2 FVC showed a similar performance with FAPAR except that its dispersion was a marginally higher.

In order to understand the potential of Sentinel-2 biophysical estimates in various applications, the performance of GMD reference maps was assessed using the same ground ESUs (Figure A2 in Appendix A). In general, our comparison reveals that GMD reference maps exhibited better performances and better relationships ($R^2(\text{LAI}_e) = 0.65$ and $R^2(\text{LAI}) = 0.79$) than Sentinel-2 estimates for LAI_e and LAI, which are primarily attributed to the use of ground ESUs in the generation of GMD reference maps. However, the performances of GMD FAPAR (RMSE = 0.11) and FVC (RMSE = 0.14) reference maps were comparable with their corresponding Sentinel-2 estimates (RMSE = 0.13 for FAPAR and 0.17 for FVC), indicating the Sentinel-2 FAPAR and FVC estimates are promising for terrestrial applications, such as coarse spatial resolution product validation, and land surface modelling, etc.

To further assess the Sentinel-2 estimates, they were compared to ground ESUs for individual vegetation types. In particular, since different crops have distinct leaf and canopy architectures, each crop type was also evaluated separately, as shown in Figure 8 and Table 3. For Sentinel-2 LAI estimates, it overestimated LAI_e and underestimated LAI for all vegetation types (especially for the crops shown in Figure 8a,b), but the specific performance over each type was quite different. The lowest uncertainty of LAI estimate was achieved by grasses (RMSE = 0.40 m²/m² for LAI_e and 0.59 m²/m² for LAI), followed by forests (RMSE = 0.69 m²/m² for LAI_e and 0.89 m²/m² for LAI) and crops (RMSE = 1.16 m²/m² for LAI_e and 1.24 m²/m² for LAI). Moreover, it can be observed that the crop types exhibited quite different performances for representing both LAI_e and LAI. The LAI estimates of corn showed the obvious overestimations (Bias = 0.96 m²/m²) and underestimations (Bias = −0.63 m²/m²) compared to ground LAI_e and LAI ESUs, introducing a large uncertainty for overall crops. The best agreement between Sentinel-2 LAI estimates and ground ESUs was achieved by coffee. For FAPAR and FVC retrievals, Sentinel-2 estimates showed a better agreement with ground ESUs over forests (lowest RMSE and highest R²) than grasses and crops. Specifically, among all crops, the FAPAR estimates of sunflower and the FVC estimates of coffee performed the best with the ground FAPAR and FVC ESUs, respectively. Even though the neural network was trained for overall vegetation types based on the description of Sentinel-2 biophysical algorithms, the performances of estimates varied with vegetation types. Additionally, it should be noted that the distribution of measurements for different vegetation types was not sufficient enough. Adding more ground ESUs, especially for the grasses, may achieve a more robust evaluation result of Sentinel-2 estimates. The various factors that contribute to the uncertainty of Sentinel-2 biophysical estimates will be further discussed in Section 5.1.

Table 3. Direct validation results of Sentinel-2 biophysical estimates over different vegetation types. The “N” and “-” denote the number of valid pixels and unavailable results, respectively. The gray color in the table indicates few ground ESUs were used to evaluate the Sentinel-2 biophysical estimates, while the bold numbers show the validation results for crops (including alfalfa, banana, Tea, ect.), forests, grasses, respectively.

Vegetation type	LAI _e (m ² /m ²)				LAI (m ² /m ²)				FAPAR				FVC			
	N	Bias	RMSE	R ²	N	Bias	RMSE	R ²	N	Bias	RMSE	R ²	N	Bias	RMSE	R ²
Alfalfa	-	-	-	-	-	-	-	-	-	-	-	-	4	−0.00	0.01	0.79
Banana	1	0.35	0.35	-	1	−0.76	0.76	-	1	−0.16	0.16	-	1	−0.24	0.24	-
Prunus Popplar	1	−0.29	0.29	-	1	−1.16	1.16	-	1	−0.10	0.10	-	1	−0.08	0.08	-
Tea	4	−0.86	1.02	<0.1	4	−1.08	1.22	<0.1	4	−0.16	0.16	0.52	4	−0.14	0.14	0.34
Coffee	7	0.59	0.64	0.73	7	0.02	0.61	0.74	7	0.01	0.15	0.92	7	−0.02	0.13	0.87
Sunflower	8	0.80	1.12	0.44	7	0.46	0.99	0.33	7	0.10	0.12	0.92	20	0.15	0.20	0.62
Soybean	24	0.40	1.23	<0.1	21	−0.29	1.47	<0.1	21	−0.08	0.17	<0.1	25	−0.08	0.19	<0.1
Corn	39	0.96	1.24	0.46	29	−0.63	1.24	0.21	30	0.02	0.12	0.33	38	0.17	0.19	0.56
Crops	84	0.65	1.16	0.37	70	−0.39	1.24	0.32	71	−0.02	0.14	0.52	100	0.06	0.18	0.34
Forests	19	0.42	0.69	0.68	19	−0.52	0.89	0.61	19	−0.04	0.07	0.63	20	−0.10	0.12	0.55
Grasses	8	0.09	0.40	0.65	8	−0.19	0.59	0.42	8	−0.03	0.14	0.39	8	−0.05	0.17	0.32

5. Discussion

5.1. Understanding Uncertainty of Sentinel-2 Biophysical Estimates

From our comprehensive evaluations presented in Section 4, the characteristics of Sentinel-2 biophysical estimates, including the RI spatial coverage and uncertainty for different vegetation types were well analyzed. Here, we investigate the possible reasons that caused the differences between retrievals and ground ESUs to better understand the performances of Sentinel-2 biophysical estimates. First, the uncertainty of estimates partially caused by the error of atmospheric correction for the surface reflectance products, which was reported by previous studies [74–76], was considered. Specifically, the range of surface reflectance uncertainty (relative uncertainty) was 0.0123 (5%)–0.0174 (14.59%) in the spectral domain of bands 3–7, 8a, 11–12. Second, uncertainties from the trained neural network used to derive the biophysical variables can also introduce some undesired errors. Based on the algorithm evaluation [34], the theoretical performance described by RMSE was 0.89 m²/m² for LAI,

0.05 for FAPAR, and 0.04 for FVC. This can explain why the FAPAR and FVC estimates showed better agreement with ground ESUs than LAI estimates. Finally, although considerable efforts were made to select the proper Sentinel-2 data with observation dates close to those of ground ESUs, the temporal gaps between these two datasets cannot be neglected. This temporal mismatch is also a very important factor that caused the potential uncertainty of Sentinel-2 biophysical estimates. For instance, the overestimation of Sentinel-2 LAI estimates compared with ground LAI_e ESUs may be due to the Sentinel-2 later observation dates. Thus, more ground measurements should be obtained in the future to improve the robustness of the validation results.

5.2. Limitations and Future Prospects

According to previous studies, the uncertainty of Sentinel-2 LAI estimates was generally 0.54–1.16 m²/m² for crops [36,37,39,46,47,50–52] and 1.55 m²/m² for forest [49]. In terms of Sentinel-2 FAPAR estimates, the uncertainty was 0.11 for crops [39] and 0.16–0.24 for forests [38]. The uncertainty of Sentinel-2 FVC estimates has been reported as being from 0.11 to 0.18 for crops [36,37,39]. Compared to these similar studies, this study used more ground validation data from the same field campaign at a large spatial scale to assess Sentinel-2 biophysical estimates. In general, our validation results agree with the findings reported by other studies. Particularly, a variety of benchmark data with the consistent measurement criteria enables us to better understand the performance of long-term Sentinel-2 estimates simultaneously for different biophysical variables (LAI, FAPAR, and FVC) and vegetation types (crops, forests, and grasses). Moreover, the uncertainties of estimates caused by the input reflectance data or the retrieval algorithm were also analyzed. However, the quantified uncertainty of Sentinel-2 biophysical estimates was limited by the availability of ground measurements, especially for the time-series validation. The most effective way is to add more ground measurements from spatiotemporally well-distributed field campaigns for various vegetation types. To achieve a robust evaluation result, an integration of in situ reference data from globally distributed research networks (i.e., FLUXNET, Chinese Ecosystem Research Network (CERN), Terrestrial Ecosystem Research Network (TERN), et al.) [25,77] will be considered in the future work because these networks have been continuously collecting in situ data for many years. The networks of site-based measurements are advantageous for the validation of decametric products because the footprint of ground measurements is close to the pixel grid of products. Therefore, more ground measurements covering the products at specific time periods (2015–present), will be collected from the global network of sites and then could be used to better quantify the uncertainties, particularly the performance of time-series attached to the Sentinel-2 biophysical estimates.

Compared to the widely used coarse-resolution (≥ 300 m) products, the first available decametric biophysical estimates can be generated from Sentinel-2 imagery by user communities as necessary. Based on the validation results, Sentinel-2 FAPAR and FVC estimates have similar performances with the corresponding GMD reference maps. However, the GMD reference maps need to collect the field measurements, which are unavailable to derive long-term or global products in this manner. Therefore, the good performances of the Sentinel-2 FAPAR and FVC estimates indicate their great potential in various applications. It should be noted that the uncertainty of Sentinel-2 LAI estimates tends to be relatively large, caused by the large uncertainty of trained neural networks. Furthermore, the algorithm improvement of Sentinel-2 biophysical estimates can be considered from several aspects. As described in Section 3.1, LAI, FAPAR, and FVC were separately derived from three independent neural networks. Therefore, the importance of input 11 variables (eight bands and three observation angles) should be calculated to better understand their performance on the retrieval of each biophysical variable. Moreover, we observed that the performance of each biophysical variable was quite different in terms of the spatial coverage of best retrievals (Figure 5) and the uncertainty (Figure 8). However, due to the highly physical correlations among LAI, FAPAR, and FVC (Figure 6), the joint retrieval of them from a neural network may improve their consistency, accuracy and computational efficiency [23], which is noteworthy to be considered in the future. Additionally, as different vegetation types exhibited a

large discrepancy in the agreement with ground measurements, the accuracy of LAI retrievals could be improved if the vegetation-specific neural network was trained. Finally, Figure 6 shows that Sentinel-2 biophysical estimates cannot well capture all the key growth stages of vegetation caused by the relative long revisit cycle of satellites and cloud contaminations. The combination of Sentinel-2 MSIs with other satellite sensors at different spatial resolutions, such as Landsat-8 OLI (Harmonized Landsat Sentinel-2) [78], Terra/Aqua MODIS, PROBA-V vegetation instrument, etc., will be promising in the generation of temporally continuous biophysical variables at a fine spatial resolution.

6. Conclusions

The current hectometric or kilometric spatial resolution biophysical products restrict the modeling of the ecosystem process at the regional level with heterogeneous landscapes. The newly developed biophysical algorithm for Sentinel-2 MSI imagery provides an effective way to generate the first global LAI, FAPAR, and FVC estimates at decametric spatial resolution. However, there is a need for a comprehensive validation of these estimates over various regions, observation dates and vegetation types to understand their performances and further extend their applications. In this study, a quantitative validation of Sentinel-2 LAI, FAPAR, and FVC estimates were performed over 2015–2016 using all ground observations with the consistent measured criteria and GMD reference maps. The results show that the accuracy of vegetation and non-vegetated classification results is more than 95% based on the ground investigations, which can be used to identify the vegetation pixel, since the algorithm generates the biophysical retrievals for all pixels. The evaluation of spatial coverage for best retrievals in different variables shows FVC estimates achieve the best performance (~ 100%) followed by LAI (87.3%) and FAPAR (87.2%) estimates. The inferior quality of other retrievals is mainly caused by the input being out of range, which needs to be considered in the future algorithm improvement. The product intercomparison shows the Sentinel-2 FAPAR and FVC estimates are quite consistent with the GMD reference maps, while large discrepancies of LAI estimates are observed over both GMD LAI_e and LAI reference maps. Confrontation with ground ESUs indicates that Sentinel-2 LAI estimates are closer to LAI_e because of uncorrected clumping effect in the retrieval algorithm. For Sentinel-2 FAPAR and FVC estimates, no obvious systematic errors (Bias = −0.02 for FAPAR and 0.03 for FVC) are observed and their uncertainties are quite low (RMSE = 0.13 for FAPAR and 0.17 for FVC). Additionally, the performances of all Sentinel-2 biophysical estimates for forests and grasses are better than for crops, even though a single neural network was used to derive estimates for all vegetation types. However, these validation results are limited due to the relatively small number of ground measurements and the temporal gaps between Sentinel-2 and ground observations. More multi-temporal ground measurements across different regions are needed to provide fundamental information for the improvement of retrieval algorithms and broad applications of these decametric biophysical estimates.

Author Contributions: Conceptualization, Q.H. and B.X.; Formal analysis, J.Y. and G.Y.; Funding acquisition, B.X. and K.L.; Investigation, J.H. and G.Y.; Methodology, Y.Z. and J.Z.; Supervision, B.X. and J.H.; Validation, J.Z. and K.L.; Writing – original draft, Q.H.; Writing – review and editing, B.X., M.S.M. and G.Y. All authors have read and agreed to the published version of the manuscript.

Funding: This research was funded by Open Fund of State Key Laboratory of Remote Sensing Science (Project No. OFSLRSS201914), National Natural Science Foundation of China (Project No. 41901380, 41971282), Fundamental Research Funds for the Central Universities (Project No. 2662018QD066, CCNU18XJ032), Sichuan Science and Technology Program (Project No. 2017JY0284), and “Innovation Ability Promotion” Program of the Sichuan Provincial Department of Finance (Project No. 2017QNJJ-023).

Acknowledgments: The Sentinel-2A Level-1C products were downloaded from the European Space Agency Copernicus Open Access Hub. We sincerely thank many field investigators for providing ground LAI, FAPAR, and FVC measurements.

Conflicts of Interest: The authors declare no conflict of interest.

Appendix A

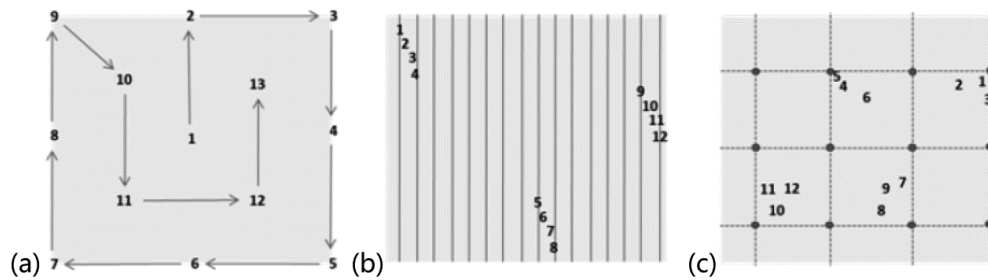


Figure A1. The examples of sampling schemes for (a) random, (b) row, and (c) regularly planted vegetation in an ESU. This figure was cited from Camacho et al. [56].

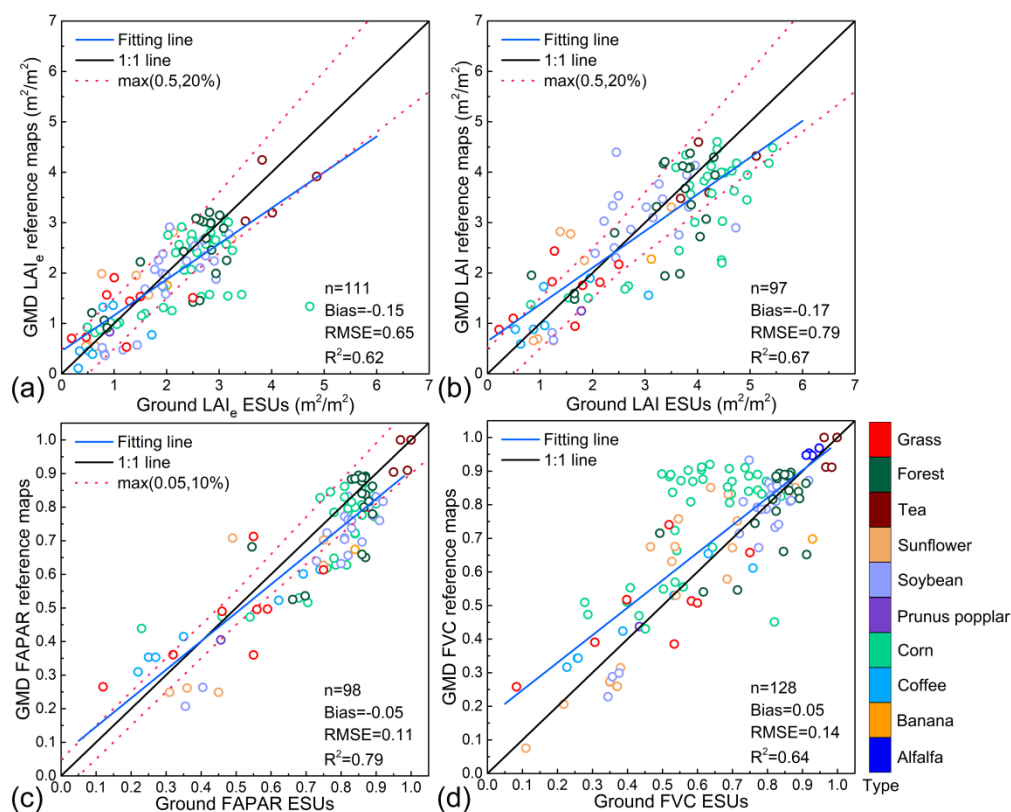


Figure A2. The comparison between ground ESUs and GMD reference maps. (a) Ground LAI_e ESUs versus GMD LAI_e reference maps; (b) Ground LAI ESUs versus GMD LAI reference maps; (c) Ground FAPAR ESUs versus GMD FAPAR reference maps; (d) Ground FVC ESUs versus GMD FVC reference maps. The colors stand for different vegetation types (i.e., crop types, forests, and grasses, respectively) shown in the right colorbar. The blue and black solid lines denote the fitting line and 1:1 line, respectively. The red dashed lines show the GCOS specifications boundaries for LAI_e (max (0.5, 20%), LAI (max (0.5, 20%)) and FAPAR (max (0.05, 10%)).

References

1. Sellers, P.J.; Dickinson, R.E.; Randall, D.A.; Betts, A.K.; Hall, F.G.; Berry, J.A.; Collatz, G.J.; Denning, A.S.; Mooney, H.A.; Nobre, C.A.; et al. Modeling the exchanges of energy, water, and carbon between continents and the atmosphere. *Science* **1997**, *275*, 502–509. [[CrossRef](#)] [[PubMed](#)]
2. Simonich, S.L.; Hites, R.A. Importance of vegetation in removing polycyclic aromatic hydrocarbons from the atmosphere. *Nature* **1994**, *370*, 49–51. [[CrossRef](#)]

3. Huang, J.; Zhuo, W.; Li, Y.; Huang, R.; Sedano, F.; Su, W.; Dong, J.; Tian, L.; Huang, Y.; Zhu, D.; et al. Comparison of three remotely sensed drought indices for assessing the impact of drought on winter wheat yield. *Int. J. Digit. Earth* **2018**, 1–23. [[CrossRef](#)]
4. Weiss, M.; Baret, F.; Garrigues, S.; Lacaze, R. LAI and fAPAR CYCLOPES global products derived from VEGETATION. Part 2: Validation and comparison with MODIS collection 4 products. *Remote Sens. Environ.* **2007**, *110*, 317–331. [[CrossRef](#)]
5. Huang, R.; Huang, J.; Zhang, C.; Ma, H.; Zhuo, W.; Chen, Y.; Zhu, D.; Wu, Q.; Mansaray, L.R. Soil temperature estimation at different depths, using remotely-sensed data. *J. Integr. Agric.* **2020**, *19*, 277–290. [[CrossRef](#)]
6. Yang, N.; Liu, D.; Feng, Q.; Xiong, Q.; Zhang, L.; Ren, T.; Zhao, Y.; Zhu, D.; Huang, J. Large-scale crop mapping based on machine learning and parallel computation with grids. *Remote Sens.* **2019**, *11*, 1500. [[CrossRef](#)]
7. Zhuo, W.; Huang, J.; Li, L.; Zhang, X.; Ma, H.; Gao, X.; Huang, H.; Xu, B.; Xiao, X. Assimilating soil moisture retrieved from Sentinel-1 and Sentinel-2 data into WOFOST model to improve winter wheat yield estimation. *Remote Sens.* **2019**, *11*, 1618. [[CrossRef](#)]
8. Chen, J.M.; Black, T.A. Defining leaf area index for non-flat leaves. *Plant Cell Environ.* **1992**, *15*, 421–429. [[CrossRef](#)]
9. Chen, J.M.; Menges, C.H.; Leblanc, S.G. Global mapping of foliage clumping index using multi-angular satellite data. *Remote Sens. Environ.* **2005**, *97*, 447–457. [[CrossRef](#)]
10. Gray, J.; Song, C. Mapping leaf area index using spatial, spectral, and temporal information from multiple sensors. *Remote Sens. Environ.* **2012**, *119*, 173–183. [[CrossRef](#)]
11. Fensholt, R.; Sandholt, I.; Rasmussen, M.S. Evaluation of MODIS LAI, fAPAR and the relation between fAPAR and NDVI in a semi-arid environment using in situ measurements. *Remote Sens. Environ.* **2004**, *91*, 490–507. [[CrossRef](#)]
12. Song, W.; Mu, X.; Ruan, G.; Gao, Z.; Li, L.; Yan, G. Estimating fractional vegetation cover and the vegetation index of bare soil and highly dense vegetation with a physically based method. *Int. J. Appl. Earth Obs. Geoinf.* **2017**, *58*, 168–176. [[CrossRef](#)]
13. Global Climate Observing System (GCOS). Systematic Observation Requirements for Satellite-Based Products for Climate, 2011 Update, Supplemental Details to the Satellite-Based Component of the Implementation Plan for the Global Observing System for Climate in Support of the UNFCCC (2010 Update). Available online: https://library.wmo.int/index.php?lvl=notice_display&id=12907 (accessed on 10 January 2020).
14. Baret, F.; Weiss, M.; Lacaze, R.; Camacho, F.; Makhmara, H.; Pacholczyk, P.; Smets, B. GEOV1: LAI and FAPAR essential climate variables and FCOVER global time series capitalizing over existing products. Part I: Principles of development and production. *Remote Sens. Environ.* **2013**, *137*, 299–309. [[CrossRef](#)]
15. Jiang, Z.; Huete, A.R.; Chen, J.; Chen, Y.; Li, J.; Yan, G.; Zhang, X. Analysis of NDVI and scaled difference vegetation index retrievals of vegetation fraction. *Remote Sens. Environ.* **2006**, *101*, 366–378. [[CrossRef](#)]
16. Jia, K.; Liang, S.; Gu, X.; Baret, F.; Wei, X.; Wang, X.; Yao, Y.; Yang, L.; Li, Y. Fractional vegetation cover estimation algorithm for Chinese GF-1 wide field view data. *Remote Sens. Environ.* **2016**, *177*, 184–191. [[CrossRef](#)]
17. Myneni, R.B.; Hoffman, S.; Knyazikhin, Y.; Privette, J.L.; Glassy, J.; Tian, Y.; Wang, Y.; Song, X.; Zhang, Y.; Smith, G.R.; et al. Global products of vegetation leaf area and fraction absorbed PAR from year one of MODIS data. *Remote Sens. Environ.* **2002**, *83*, 214–231. [[CrossRef](#)]
18. Baret, F.; Hagolle, O.; Geiger, B.; Bicheron, P.; Miras, B.; Huc, M.; Berthelot, B.; Niño, F.; Weiss, M.; Samain, O.; et al. LAI, fAPAR and fCover CYCLOPES global products derived from VEGETATION: Part 1: Principles of the algorithm. *Remote Sens. Environ.* **2007**, *110*, 275–286. [[CrossRef](#)]
19. Yan, K.; Park, T.; Yan, G.; Chen, C.; Yang, B.; Liu, Z.; Nemani, R.; Knyazikhin, Y.; Myneni, R. Evaluation of MODIS LAI/FPAR product Collection 6. Part 1: Consistency and improvements. *Remote Sens.* **2016**, *8*, 359. [[CrossRef](#)]
20. Campos-Taberner, M.; Moreno-Martínez, Á.; García-Haro, F.; Camps-Valls, G.; Robinson, N.; Kattge, J.; Running, S. Global estimation of biophysical variables from Google Earth Engine platform. *Remote Sens.* **2018**, *10*, 1167. [[CrossRef](#)]
21. Ganguly, S.; Samanta, A.; Schull, M.A.; Shabanov, N.V.; Milesi, C.; Nemani, R.R.; Knyazikhin, Y.; Myneni, R.B. Generating vegetation leaf area index Earth system data record from multiple sensors. Part 2: Implementation, analysis and validation. *Remote Sens. Environ.* **2008**, *112*, 4318–4332. [[CrossRef](#)]

22. Zhu, Z.; Bi, J.; Pan, Y.; Ganguly, S.; Anav, A.; Xu, L.; Samanta, A.; Piao, S.; Nemani, R.R.; Myneni, B.R. Global data sets of vegetation leaf area index (LAI)_{3g} and fraction of photosynthetically active radiation (FPAR)_{3g} derived from global inventory modeling and mapping studies (GIMMS) normalized difference vegetation index (NDVI)_{3g} for the period 1981 to 2011. *Remote Sens.* **2013**, *5*, 927–948.
23. García-Haro, F.J.; Campos-Taberner, M.; Muñoz-Marí, J.; Laparra, V.; Camacho, F.; Sánchez-Zapero, J.; Camps-Valls, G. Derivation of global vegetation biophysical parameters from EUMETSAT Polar System. *ISPRS J. Photogramm. Remote Sens.* **2018**, *139*, 57–74. [[CrossRef](#)]
24. Claverie, M.; Matthews, L.J.; Vermote, F.E.; Justice, O.C. A 30+ year AVHRR LAI and FAPAR climate data record: Algorithm description and validation. *Remote Sens.* **2016**, *8*, 263. [[CrossRef](#)]
25. Xu, B.; Park, T.; Yan, K.; Chen, C.; Zeng, Y.; Song, W.; Yin, G.; Li, J.; Liu, Q.; Knyazikhin, Y.; et al. Analysis of global LAI/FPAR products from VIIRS and MODIS sensors for spatio-temporal consistency and uncertainty from 2012–2016. *Forests* **2018**, *9*, 73. [[CrossRef](#)]
26. Yan, K.; Park, T.; Chen, C.; Xu, B.; Song, W.; Yang, B.; Zeng, Y.; Liu, Z.; Yan, G.; Knyazikhin, Y.; et al. Generating global products of LAI and FPAR from SNPP-VIIRS data: Theoretical background and implementation. *IEEE Trans. Geosci. Remote Sens.* **2018**, *56*, 2119–2137. [[CrossRef](#)]
27. Li, W.; Weiss, M.; Waldner, F.; Defourny, P.; Demarez, V.; Morin, D.; Hagolle, O.; Baret, F. A generic algorithm to estimate LAI, FAPAR and FCOVER variables from SPOT4 HRVIR and Landsat sensors: Evaluation of the consistency and comparison with ground measurements. *Remote Sens.* **2015**, *7*, 15494–15516. [[CrossRef](#)]
28. Ganguly, S.; Nemani, R.R.; Zhang, G.; Hashimoto, H.; Milesi, C.; Michaelis, A.; Wang, W.; Votava, P.; Samanta, A.; Melton, F.; et al. Generating global leaf area index from Landsat: Algorithm formulation and demonstration. *Remote Sens. Environ.* **2012**, *122*, 185–202. [[CrossRef](#)]
29. Chen, J.M.; Pavlic, G.; Brown, L.; Cihlar, J.; Leblanc, S.G.; White, H.P.; Hall, R.J.; Peddle, D.R.; King, D.J.; Trofymow, J.A.; et al. Derivation and validation of Canada-wide coarse-resolution leaf area index maps using high-resolution satellite imagery and ground measurements. *Remote Sens. Environ.* **2002**, *80*, 165–184. [[CrossRef](#)]
30. Yin, G.; Li, J.; Liu, Q.; Li, L.; Zeng, Y.; Xu, B.; Yang, L.; Zhao, J. Improving leaf area index retrieval over heterogeneous surface by integrating textural and contextual information: A case study in the Heihe river basin. *IEEE Geosci. Remote Sens. Lett.* **2015**, *12*, 359–363.
31. Xu, B.; Li, J.; Park, T.; Liu, Q.; Zeng, Y.; Yin, G.; Yan, K.; Chen, C.; Zhao, J.; Fan, W.; et al. Improving leaf area index retrieval over heterogeneous surface mixed with water. *Remote Sens. Environ.* **2020**, *240*, 111700. [[CrossRef](#)]
32. Fang, H.; Li, W.; Myneni, R. The impact of potential land cover misclassification on MODIS leaf area index (LAI) estimation: A statistical perspective. *Remote Sens.* **2013**, *5*, 830–844. [[CrossRef](#)]
33. Drusch, M.; Del Bello, U.; Carlier, S.; Colin, O.; Fernandez, V.; Gascon, F.; Hoersch, B.; Isola, C.; Laberinti, P.; Martimort, P.; et al. Sentinel-2: ESA's optical high-resolution mission for GMES operational services. *Remote Sens. Environ.* **2012**, *120*, 25–36. [[CrossRef](#)]
34. Weiss, M.; Baret, F. S2ToolBox Level 2 Products: LAI, FAPAR, FCOVER. Version 1.1. 2016. Available online: http://step.esa.int/docs/extra/ATBD_S2ToolBox_L2B_V1.1.pdf (accessed on 21 October 2019).
35. Colombo, R.; Bellingeri, D.; Fasolini, D.; Marino, C.M. Retrieval of leaf area index in different vegetation types using high resolution satellite data. *Remote Sens. Environ.* **2003**, *86*, 120–131. [[CrossRef](#)]
36. Djamai, N.; Zhong, D.; Fernandes, R.; Zhou, F. Evaluation of vegetation biophysical variables time series derived from synthetic Sentinel-2 images. *Remote Sens.* **2019**, *11*, 1547. [[CrossRef](#)]
37. Djamai, N.; Fernandes, R.; Weiss, M.; McNairn, H.; Goita, K. Validation of the Sentinel Simplified Level 2 Product Prototype Processor (SL2P) for mapping cropland biophysical variables using Sentinel-2/MSI and Landsat-8/OLI data. *Remote Sens. Environ.* **2019**, *225*, 416–430. [[CrossRef](#)]
38. Putzenlechner, B.; Castro, S.; Kiese, R.; Ludwig, R.; Marzahn, P.; Sharp, I.; Sanchez-Azofeifa, A. Validation of Sentinel-2 fAPAR products using ground observations across three forest ecosystems. *Remote Sens. Environ.* **2019**, *232*, 111310. [[CrossRef](#)]
39. Upreti, D.; Huang, W.; Kong, W.; Pascucci, S.; Pignatti, S.; Zhou, X.; Ye, H.; Casa, R. A comparison of hybrid machine learning algorithms for the retrieval of wheat biophysical variables from Sentinel-2. *Remote Sens.* **2019**, *11*, 481. [[CrossRef](#)]
40. Fang, H.; Wei, S.; Liang, S. Validation of MODIS and CYCLOPES LAI products using global field measurement data. *Remote Sens. Environ.* **2012**, *119*, 43–54. [[CrossRef](#)]

41. Xu, B.; Li, J.; Liu, Q.; Huete, A.; Yu, Q.; Zeng, Y.; Yin, G.; Zhao, J.; Yang, L. Evaluating spatial representativeness of station observations for remotely sensed leaf area index products. *IEEE J. Sel. Top. Appl. Earth Obs. Remote Sens.* **2016**, *9*, 3267–3282. [[CrossRef](#)]
42. Camacho, F.; Cernicharo, J.; Lacaze, R.; Baret, F.; Weiss, M. GEOV1: LAI, FAPAR essential climate variables and FCOVER global time series capitalizing over existing products. Part 2: Validation and intercomparison with reference products. *Remote Sens. Environ.* **2013**, *137*, 310–329. [[CrossRef](#)]
43. Garrigues, S.; Lacaze, R.; Baret, F.; Morisette, J.T.; Weiss, M.; Nickeson, J.E.; Fernandes, R.; Plummer, S.; Shabanov, N.V.; Myneni, R.B.; et al. Validation and intercomparison of global leaf area index products derived from remote sensing data. *J. Geophys. Res.* **2008**, *113*, G02028. [[CrossRef](#)]
44. Claverie, M.; Vermote, E.F.; Weiss, M.; Baret, F.; Hagolle, O.; Demarez, V. Validation of coarse spatial resolution LAI and FAPAR time series over cropland in southwest France. *Remote Sens. Environ.* **2013**, *139*, 216–230. [[CrossRef](#)]
45. Yin, G.; Li, A.; Jin, H.; Zhao, W.; Bian, J.; Qu, Y.; Zeng, Y.; Xu, B. Derivation of temporally continuous LAI reference maps through combining the LAINet observation system with CACAO. *Agric. For. Meteorol.* **2017**, *233*, 209–221. [[CrossRef](#)]
46. Campos-Taberner, M.; García-Haro, J.F.; Camps-Valls, G.; Grau-Muedra, G.; Nutini, F.; Busetto, L.; Katsantonis, D.; Stavrakoudis, D.; Minakou, C.; Gatti, L.; et al. Exploitation of SAR and optical Sentinel data to detect rice crop and estimate seasonal dynamics of leaf area index. *Remote Sens.* **2017**, *9*, 248. [[CrossRef](#)]
47. Campos-Taberner, M.; Javier Garcia-Haro, F.; Busetto, L.; Ranghetti, L.; Martinez, B.; Amparo Gilabert, M.; Camps-Valls, G.; Camacho, F.; Boschetti, M. A critical comparison of remote sensing leaf area index estimates over rice-cultivated areas: From Sentinel-2 and Landsat-7/8 to MODIS, GEOV1 and EUMETSAT Polar System. *Remote Sens.* **2018**, *10*, 763. [[CrossRef](#)]
48. Korhonen, L.; Packalen, P.; Rautiainen, M. Comparison of Sentinel-2 and Landsat 8 in the estimation of boreal forest canopy cover and leaf area index. *Remote Sens. Environ.* **2017**, *195*, 259–274. [[CrossRef](#)]
49. Brown, A.L.; Ogotu, O.B.; Dash, J. Estimating forest leaf area index and canopy chlorophyll content with Sentinel-2: An evaluation of two hybrid retrieval algorithms. *Remote Sens.* **2019**, *11*, 1752. [[CrossRef](#)]
50. Pan, H.; Chen, Z.; Ren, J.; Li, H.; Wu, S. Modeling winter wheat leaf area index and canopy water content with three different approaches using Sentinel-2 multispectral instrument data. *IEEE J. Sel. Top. Appl. Earth Obs. Remote Sens.* **2019**, *12*, 482–492. [[CrossRef](#)]
51. Pasqualotto, N.; D’Urso, G.; Bolognesi, F.S.; Belfiore, R.O.; Van Wittenberghe, S.; Delegido, J.; Pezzola, A.; Winschel, C.; Moreno, J. Retrieval of evapotranspiration from Sentinel-2: Comparison of vegetation indices, semi-empirical models and SNAP biophysical processor approach. *Agronomy* **2019**, *9*, 663. [[CrossRef](#)]
52. Pasqualotto, N.; Delegido, J.; Van Wittenberghe, S.; Rinaldi, M.; Moreno, J. Multi-crop green LAI estimation with a new simple sentinel-2 LAI index (SeLI). *Sensors* **2019**, *19*, 904. [[CrossRef](#)]
53. Camacho, F.; Lacaze, R.; Latorre, C.; Baret, F.; De la Cruz, F.; Demarez, V.; Di Bella, C.; García-Haro, J.; González-Dugo, M.P.; Kussul, N. Collection of ground biophysical measurements in support of Copernicus Global Land Product Validation: The ImagineS database. In Proceedings of the EGU General Assembly, Vienna, Austria, 17–22 April 2015; Volume 17. Geophysical Research Abstracts, 17 EGU2015–2209-1.
54. Beck, H.E.; Zimmermann, N.E.; McVicar, T.R.; Vergopolan, N.; Berg, A.; Wood, E.F. Present and future Köppen-Geiger climate classification maps at 1-km resolution. *Sci. Data* **2018**, *5*, 180214. [[CrossRef](#)] [[PubMed](#)]
55. Camacho, F.; Lacaze, R.; Latorre, C.; Baret, F.; De la Cruz, F.; Demarez, V.; Di Bella, C.; Fang, H.; García-Haro, J.; Gonzalez, M.P. A network of sites for ground biophysical measurements in support of Copernicus Global Land Product Validation. In Proceedings of the IV RAQRS Conference, Torrent, Spain, 22–26 September 2014; pp. 22–26.
56. Camacho, F.; Latorre, C.; Roujean, J.L. Vegetation field data and production of ground-based maps. In Proceedings of the AHSPECT Multi-Site Campaign, South West, France, 22–25 June 2015.
57. Fang, H.; Li, W.; Wei, S.; Jiang, C. Seasonal variation of leaf area index (LAI) over paddy rice fields in NE China: Intercomparison of destructive sampling, LAI-2200, digital hemispherical photography (DHP), and AccuPAR methods. *Agric. For. Meteorol.* **2014**, *198–199*, 126–141. [[CrossRef](#)]
58. Weiss, M.; Baret, F. *Can_Eye V6.4.91 User Manual*; French National Institute for Agriculture Research (INRA): Toulouse, France, 2017.

59. Liu, C.C.; Zhang, Y.C.; Chen, P.Y.; Lai, C.C.; Chen, Y.H.; Cheng, J.H.; Ko, M.H. Clouds classification from Sentinel-2 imagery with deep residual learning and semantic image segmentation. *Remote Sens.* **2019**, *11*, 119. [[CrossRef](#)]
60. Jacquemoud, S.; Verhoef, W.; Baret, F.; Bacour, C.; Zarco-Tejada, P.J.; Asner, G.P.; François, C.; Ustin, S.L. PROSPECT + SAIL models: A review of use for vegetation characterization. *Remote Sens. Environ.* **2009**, *113*, S56–S66. [[CrossRef](#)]
61. Verhoef, W. Light scattering by leaf layers with application to canopy reflectance modeling: The SAIL model. *Remote Sens. Environ.* **1984**, *16*, 125–141. [[CrossRef](#)]
62. Jacquemoud, S.; Baret, F. PROSPECT: A model of leaf optical properties spectra. *Remote Sens. Environ.* **1990**, *34*, 75–91. [[CrossRef](#)]
63. Jacquemoud, S.; Baret, F.; Hanocq, J.F. Modeling spectral and bidirectional soil reflectance. *Remote Sens. Environ.* **1992**, *41*, 123–132. [[CrossRef](#)]
64. Liu, W.; Baret, F.; Gu, X.; Tong, Q.; Zheng, L.; Zhang, B. Relating soil surface moisture to reflectance. *Remote Sens. Environ.* **2002**, *81*, 238–246.
65. Baret, F.; de Solan, B.; Lopez-Lozano, R.; Ma, K.; Weiss, M. GAI estimates of row crops from downward looking digital photos taken perpendicular to rows at 57.5° zenith angle: Theoretical considerations based on 3D architecture models and application to wheat crops. *Agric. For. Meteorol.* **2010**, *150*, 1393–1401. [[CrossRef](#)]
66. Wang, Y.J.; Tian, Y.H.; Zhang, Y.; El-Saleous, N.; Knyazikhin, Y.; Vermote, E.; Myneni, R.B. Investigation of product accuracy as a function of input and model uncertainties: Case study with SeaWiFS and MODIS LAI/FPAR algorithm. *Remote Sens. Environ.* **2001**, *78*, 299–313. [[CrossRef](#)]
67. Baghzouz, M.; Devitt, D.A.; Fenstermaker, L.F.; Young, M.H. Monitoring vegetation phenological cycles in two different semi-arid environmental settings using a ground-based NDVI system: A potential approach to improve satellite data interpretation. *Remote Sens.* **2010**, *2*, 990–1013. [[CrossRef](#)]
68. Candiago, S.; Remondino, F.; De Giglio, M.; Dubbini, M.; Gattelli, M. Evaluating multispectral images and vegetation indices for precision farming applications from UAV images. *Remote Sens.* **2015**, *7*, 4026–4047. [[CrossRef](#)]
69. Hmimina, G.; Dufrène, E.; Pontailier, J.Y.; Delpierre, N.; Aubinet, M.; Caquet, B.; de Grandcourt, A.; Burban, B.; Flechard, C.; Granier, A.; et al. Evaluation of the potential of MODIS satellite data to predict vegetation phenology in different biomes: An investigation using ground-based NDVI measurements. *Remote Sens. Environ.* **2013**, *132*, 145–158. [[CrossRef](#)]
70. Soudani, K.; Hmimina, G.; Delpierre, N.; Pontailier, J.Y.; Aubinet, M.; Bonal, D.; Caquet, B.; de Grandcourt, A.; Burban, B.; Flechard, C.; et al. Ground-based network of NDVI measurements for tracking temporal dynamics of canopy structure and vegetation phenology in different biomes. *Remote Sens. Environ.* **2012**, *123*, 234–245. [[CrossRef](#)]
71. Brantley, S.T.; Zinnert, J.C.; Young, D.R. Application of hyperspectral vegetation indices to detect variations in high leaf area index temperate shrub thicket canopies. *Remote Sens. Environ.* **2011**, *115*, 514–523. [[CrossRef](#)]
72. Tillack, A.; Clasen, A.; Kleinschmit, B.; Foerster, M. Estimation of the seasonal leaf area index in an alluvial forest using high-resolution satellite-based vegetation indices. *Remote Sens. Environ.* **2014**, *141*, 52–63. [[CrossRef](#)]
73. Zhou, X.; Zheng, H.B.; Xu, X.Q.; He, J.Y.; Ge, X.K.; Yao, X.; Cheng, T.; Zhu, Y.; Cao, W.X.; Tian, Y.C. Predicting grain yield in rice using multi-temporal vegetation indices from UAV-based multispectral and digital imagery. *ISPRS J. Photogramm. Remote Sens.* **2017**, *130*, 246–255. [[CrossRef](#)]
74. Djamaï, N.; Fernandes, R. Comparison of SNAP-derived Sentinel-2A L2A product to ESA product over Europe. *Remote Sens.* **2018**, *10*, 926. [[CrossRef](#)]
75. Li, Y.; Chen, J.; Ma, Q.; Zhang, H.K.; Liu, J. Evaluation of Sentinel-2A surface reflectance derived using Sen2Cor in North America. *IEEE J. Sel. Top. Appl. Earth Obs. Remote Sens.* **2018**, *11*, 1997–2021. [[CrossRef](#)]
76. Martins, S.V.; Barbosa, C.C.; De Carvalho, A.L.; Jorge, S.D.; Lobo, D.F.; Novo, M.E. Assessment of atmospheric correction methods for Sentinel-2 MSI images applied to Amazon floodplain lakes. *Remote Sens.* **2017**, *9*, 322. [[CrossRef](#)]

77. Xu, B.; Li, J.; Park, T.; Liu, Q.; Zeng, Y.; Yin, G.; Zhao, J.; Fan, W.; Yang, L.; Knyazikhin, Y.; et al. An integrated method for validating long-term leaf area index products using global networks of site-based measurements. *Remote Sens. Environ.* **2018**, *209*, 134–151. [[CrossRef](#)]
78. Claverie, M.; Ju, J.; Masek, J.G.; Dungan, J.L.; Vermote, E.F.; Roger, J.-C.; Skakun, S.V.; Justice, C. The Harmonized Landsat and Sentinel-2 surface reflectance data set. *Remote Sens. Environ.* **2018**, *219*, 145–161. [[CrossRef](#)]



© 2020 by the authors. Licensee MDPI, Basel, Switzerland. This article is an open access article distributed under the terms and conditions of the Creative Commons Attribution (CC BY) license (<http://creativecommons.org/licenses/by/4.0/>).